1

2 **Simulating Coupled Surface-Subsurface Flows with ParFlow v3.5.0: Capabilities,**
3 **applications, and ongoing development of an open-source, massively parallel, integrated**
4 **hydrologic model**

5

6

7

8 Benjamin N. O. Kuffour[1,*], Nicholas B. Engdahl[1], Carol S. Woodward[2],

9 Laura E. Condon[3], Stefan Kollet[4,5], and Reed M. Maxwell[6]

10

11

12 [1]Civil and Environmental Engineering, Washington State University, Pullman, WA, USA

13 [2]Center for Applied Scientific Computing, Lawrence Livermore National Laboratory, Livermore,
14 CA, USA

15 [3]Hydrology and Atmospheric Sciences, University of Arizona, Tucson, AZ, USA

16 [4]Institute for Bio- and Geosciences, Agrosphere (IBG-3), Research Centre Jülich, Geoverbund
17 ABC/J, Jülich

18 [5]Centre for High-Performance Scientific Computing in Terrestrial Systems, Geoverbund ABC/J,
19 Jülich

20 [6]Integrated GroundWater Modeling Center and Department of Geology and Geological
21 Engineering, Colorado School of Mines, Golden, CO, USA

22

23 *Correspondence to:* Benjamin N. O. Kuffour (b.kuffour@wsu.edu)

24

25

26

1

27   Abstract

28   Surface and subsurface flow constitute a naturally linked hydrologic continuum that has not

29   traditionally been simulated in an integrated fashion. Recognizing the interactions between these

30   systems has encouraged the development of integrated hydrologic models (IHMs) capable of

31   treating surface and subsurface systems as a single integrated resource. IHMs is dynamically

32   evolving with improvement in technology and the extent of their current capabilities are often only

33   known to the developers and not general users. This article provides an overview of the core

34   functionality, capability, applications, and ongoing development of one open-source IHM,

35   ParFlow. ParFlow is a parallel, integrated, hydrologic model that simulates surface and subsurface

36   flows. ParFlow solves Richards' equation for three-dimensional variably saturated groundwater

37   flow and the two-dimensional kinematic wave approximation of the shallow water equations for

38   overland flow. The model employs a conservative centered finite difference scheme and a

39   conservative finite volume method for subsurface flow and transport, respectively. ParFlow uses

40   multigrid preconditioned Krylov and Newton-Krylov methods to solve the linear and nonlinear

41   systems within each time step of the flow simulations. The code has demonstrated very efficient

42   parallel solution capabilities. ParFlow has been coupled to geochemical reaction, land surface

43   (e.g. Common Land Model), and atmospheric models to study the interactions among the

44   subsurface, land surface, and the atmosphere systems across different spatial scales. This overview

45   focuses on the current capabilities of the code, the core simulation engine, and the primary

46   couplings of the subsurface model to other codes, taking a high-level perspective.

47

48

Geoscientific
Model Development
Discussions

49   1. Introduction

50   Surface and subsurface (unsaturated and saturated zones) water are connected components of

51   a hydrologic continuum (Kumar et al., 2009) . The recognition that flow systems (i.e. surface and

52   subsurface) are a single integrated resource has stimulated the development of integrated

53   hydrologic models (IHMs), which include codes like ParFlow (Ashby and Falgout, 1996; Kollet

54   and Maxwell, 2006) , HydroGeoSphere (Therrien and Sudicky, 1996), PIHM (Kumar, 2009), and

55   CATHY (Camporese et al., 2010) . These codes explicitly simulate different hydrological

56   processes such as feedbacks between processes that affect the timing and rates of

57   evapotranspiration, vadose flow, surface runoff and groundwater interactions. That is, IHMs are

58   designed specifically to include the interactions between traditionally incompatible process

59   domains (e.g. groundwater and land surface flow) (Engdahl and Maxwell, 2015) . Most IHMs

60   adopt a similar, physically-based approach to describe watershed dynamics where the governing

61   equations of three–dimensional variably saturated subsurface flow are coupled to shallow water

62   equations for surface runoff. The advantage of the coupled approach is that it allows hydraulically-

63   linked interconnected groundwater–surface water systems to evolve dynamically, and for natural

64   feedbacks between the components to develop (Sulis et al., 2010; Maxwell et al., 2011; Weill et

65   al., 2011; Williams and Maxwell, 2011; Simmer et al., 2015). A large body of literature now exists

66   presenting applications of the various IHMs to solve hydrologic questions. Each model has its own

67   technical documentation, but the individual development, maintenance, and sustainability efforts

68   differ between tools. Some IHMs represent commercial investments and others are community,

69   open-sourced projects, but all are dynamically evolving as technology improves and new features

70   are added. Consequently, it can be difficult to answer the question of "what exactly can this IHM

71   do today" without navigating dense user documentation. The purpose of this manuscript is to

72   provide a current review of the functions, capabilities, and ongoing development of one of the

73   open-source integrated models, ParFlow, in a format that is more accessible to a broad audience

74   than a user manual or articles detailing specific applications of the model.

75   ParFlow is a parallel integrated hydrologic model that simulates surface, unsaturated, and

76   groundwater flow (Maxwell et al., 2016). ParFlow computes fluxes through the subsurface, as well

77   as interactions with above-ground or surface and overland flow: all driven by gradients in

78   hydraulic head. Richards' equation is employed to simulate variably saturated three-dimensional

79   groundwater flow (Richards, 1931). Overland flow can be generated by saturation or infiltration

80   excess using a free surface overland flow boundary condition combined with Manning's equation

81   and the kinematic wave formulations of the dynamic wave equation (Kollet and Maxwell, 2006).

82   ParFlow solves these governing equations employing either a fully coupled or integrated approach

83   where surface and subsurface flows are solved simultaneously the Richards' equation in three-

84   dimensional form (Gilbert and Maxwell, 2016) , or an indirect approach where the different

85   components can be partitioned and flows in only one of the systems (surface or subsurface flows)

86   is solved. For the groundwater flow solution, ParFlow makes use of an implicit backward Euler

87   scheme in time, and a cell-centered finite-difference scheme in space (Woodward, 1998). An

88   upwind finite-volume scheme in space and an implicit backward Euler scheme in time is used for

89   the overland flow component (Maxwell et al., 2007). ParFlow uses Krylov linear solvers with

90   multigrid preconditioners for the flow equations along with a Newton method for the nonlinearities

91   in the variably saturated flow system (Ashby and Falgout, 1996; Jones and Woodward, 2001).

92   ParFlow's physically based approach requires a number of parameterizations e.g. subsurface

93   hydraulic properties, such as porosity, the saturated hydraulic conductivity, and the pressure-

94   saturation relationship parameters (relative permeability), etc. (Kollet et al., 2010).

95   ParFlow is well documented and has been applied to surface and subsurface flow problems

96   including simulating the dynamic nature of groundwater and surface-subsurface interconnectivity

97   in large domains (e.g. Kollet and Maxwell, 2008; Ferguson and Maxwell, 2012; Condon et al.,

98   2013; Condon and Maxwell, 2014), small catchments (Ashby et al., 1994; Kollet and Maxwell,

99   2006; Engdahl et al., 2016), complex terrain with highly heterogenous subsurface permeability

100   (e.g. Engdahl and Maxwell, 2015; Kollet et al., 2017), large watersheds (Abu-El-Sha'r and Rihani,

101   2007; Kollet et al., 2010), continental scale flows (Condon et al., 2015; Maxwell et al., 2015) and

102   even subsurface–surface and –atmospheric coupling (Maxwell et al., 2011; Williams and Maxwell,

103   2011; Williams et al., 2013; Gasper et al., 2014; Shrestha et al., 2015). The rest of the paper is

104   organized as follows: We provide a brief history of ParFlow's development in Section 1.1. In

105   Section 2, we describe the core functionality of the code, i.e. the primary functions and the model

106   equations and grid type used by ParFlow. Section 3 covers equation discretization and solvers (e.g.

107   inexact Newton-Krylov, the ParFlow Multigrid (PFMG) preconditioner, and the Multigrid-

108   Preconditioned Conjugate Gradient (MGCG) method) used in ParFlow. Examples of parallel

109   scaling and performance efficiency of ParFlow are revisited in Section 4. The coupling capabilities

110   of ParFlow, with other atmospheric, land surface, and subsurface models are shown in Section 5.

111   We provide a summary and discussion, future directions to the development of ParFlow, and give

112   some concluding remarks in Section 6.

113   1.1 Development History

114   ParFlow development commenced as part of an effort to develop an open–source, object–

115   oriented, parallel watershed flow model initiated by scientists from the Center for Applied

116   Scientific Computing (CASC), Environmental Programs, and the Environmental Protection

117   Department at the Lawrence Livermore National Laboratory (LLNL) in the mid–1990s. ParFlow

118   was born out of this effort to address the need for a code that combines fast, nonlinear solution

119   schemes with massively parallel processing power, and its development continues today (e.g.

120   Ashby et al., 1993; Smith et al., 1995; Woodward, 1998; Maxwell and Miller, 2005; Kollet and

121   Maxwell, 2008; Rihani et al., 2010; Simmer et al., 2015). ParFlow, is now a collaborative effort

122   between numerous institutions including Colorado School of Mines, Research Center Jülich,

123   University of Bonn, Washington State University, the University of Arizona, and Lawrence

124   Livermore National Laboratory, and its working base and development community continues to

125   expand.

126   ParFlow was originally developed for modeling saturated fluid flow and chemical transport

127   in three-dimensional heterogeneous media. Over the past few decades, ParFlow underwent several

128   modifications and expansions (i.e. additional features and capabilities have been implemented)

129   and has seen an exponential growth of applications. For example, a two-dimensional distributed

130   overland flow simulator (surface water component) was implemented into ParFlow (Kollet and

131   Maxwell, 2006) to simulate interaction between surface and subsurface flows. Such additional

132   implementations have resulted in improved numerical methods in the code. In recent times,

133   ParFlow has been used in several coupling studies, with subsurface, land surface, and atmospheric

134   models to include physical processes at the land surface (Maxwell and Miller, 2005; Maxwell et

135   al., 2007, 2011; Kollet, 2009; Williams and Maxwell, 2011; Valcke et al., 2012; Valcke, 2013;

136   Shrestha et al., 2014; Beisman et al., 2015) across different spatial scales and resolutions (Kollet

137   and Maxwell, 2008; Condon and Maxwell, 2015; Maxwell et al., 2015). Also, a terrain following

138   mesh formulation has been implemented (Maxwell, 2013) that allows ParFlow to handle problems

139   with fine space discretization near the ground surface (these are discussed in detail below).

140

141   2. Core Functionality of ParFlow

142   The core functionality of the ParFlow model is the solution of three-dimensional variably

143   saturated groundwater flow in heterogeneous porous media ranging from simple domains with

144   minimal topography and/or heterogeneity to highly resolved continental-scale catchments (Jones

145   and Woodward, 2001; Maxwell and Miller, 2005; Kollet and Maxwell, 2008; Maxwell, 2013).

146   Within this range of complexity, the ParFlow model can operate in three different modes: 1).

147   variably saturated; 2). steady–state saturated; and 3). integrated–watershed flows; however, all

148   these modes share a common sparse coefficient matrix solution framework.

149   2.1 Variably Saturated Flow

Geoscientific
Model Development
Discussions
Open Access
EGU

150   ParFlow can operate in variably saturated mode using the well-known, mixed form of

151   Richards' equation (Celia et al., 1990). The mixed form of Richards' equation implemented in

152   ParFlow is:

$$S_s S_w(p) \frac{\partial p}{\partial t} + \phi \frac{\partial (S_w(p))}{\partial t} = \nabla . \boldsymbol{q} + q_s, \qquad (1)$$

$$\boldsymbol{q} = -k_s(x) k_r(p) \nabla(p - z), \qquad (2)$$

155   where S_s is the specific storage coefficient $[\text{L}^{-1}]$, S_w is the relative of saturation $[-]$ as a function

156   of pressure head p of the fluid/water $[\text{L}]$, t is time $[\text{T}]$, ϕ is the porosity of the medium $[-]$, $\boldsymbol{q}$ is

157   the specific volumetric (Darcy) flux $[\text{LT}^{-1}]$, $k_s(x)$ is the saturated hydraulic conductivity tensor

158    $[\text{LT}^{-1}]$, k_r is the relative permeability $[-]$ which is a function of pressure head, q_s is the general

159   source/sink term $[\text{L}^3\text{T}^{-1}]$ (includes wells and surface fluxes e.g. evaporation and transpiration),

160   and z is depth below the surface $[\text{L}]$. The Richards' equation assumes that the air phase is infinitely

161   mobile (Richards, 1931). ParFlow has been used to numerically simulate river-aquifer exchange

162   (free-surface flow and subsurface flow), (Frei et al., 2009), and highly heterogenous problems

163   under variably-saturated flow conditions (Woodward, 1998; Jones and Woodward, 2001; Kollet

164   et al., 2010). Under saturated conditions e.g. simulating linear groundwater movement under

165   assumed predevelopment conditions, the steady-state saturated mode can be used.

166

167   2.2 Steady–State Saturated Flow

168   The most basic operational mode is the solution of the steady state, fully saturated

169   groundwater flow equation:

170 $$\nabla . \boldsymbol{q} - q_s = 0, \qquad\qquad (3)$$

171 where q_s represents a general source/sink term e.g. wells $[\mathrm{L}^3\mathrm{T}^{-1}]$, $\boldsymbol{q}$ is the Darcy' flux $[\mathrm{L}^2\mathrm{T}^{-1}]$

172 which is usually written as:

173 $$\boldsymbol{q} = -k_s \nabla p \qquad\qquad (4)$$

174 where k_s is the saturated hydraulic conductivity $[\mathrm{LT}^{-1}]$ and p represents the 3-D hydraulic head-

175 potential [L]. When studying sophisticated or complex phenomena e.g. simulating fully coupled

176 system (i.e. surface and subsurface flow), an overland flow boundary condition is employed.

177

178 2.3 Overland Flow

179   Surface water systems are connected to the subsurface, and these interactions are

180 particularly important for rivers. However, these connections have been historically difficult to

181 represent explicitly in numerical simulations. A common approach has been to use river routing

182 codes, like HEC, and MODFLOW and its River Package to determine head in the river, which is

183 then used as a boundary condition for the subsurface model. This approach prevents feedbacks

184 between the two models, and a better representation of the physical processes in these kinds of

185 problems is one of the motivations for IHMs. Overland flow is implemented in ParFlow as a two–

186 dimensional kinematic wave equation approximation of the shallow water equations. The

187 continuity equation for two-dimensional shallow overland flow is given as;

188 $$\frac{\partial \psi_s}{\partial t} = \nabla . (\vec{v} \psi_s) + q_s, \qquad\qquad (5)$$

189   where $\vec{v}$ is the depth averaged velocity vector $[\mathrm{LT}^{-1}]$, ψ_s is the surface ponding depth $[\mathrm{L}]$, t is time

190     $[\mathrm{T}]$, and q_s is a general source/sink (e.g. precipitation rate) $[\mathrm{LT}^{-1}]$. Ignoring the dynamic and

191   diffusion terms results in the momentum equation

192     $$S_{f,i} = S_{o,i}, \tag{6}$$

193   which is known as the kinematic wave approximation. The $S_{f,i}$ and $S_{o,i}$ represent the friction $[-]$

194   and bed (gravity forcing term) $[-]$ slopes respectively, where i indicates $x-$ and $y-$ directions

195   (also shown in equations 7 and 8) (Maxwell et al., 2015). Manning's equation is used to generate

196   a flow depth–discharge relationship:

197     $$v_x = \frac{\sqrt{S_{f,x}}}{n}\psi_s^{2/3}, \text{ and} \tag{7}$$

198     $$v_y = \frac{\sqrt{S_{f,y}}}{n}\psi_s^{2/3} \tag{8}$$

199   where n is the Manning's roughness coefficient $\left[\mathrm{TL}^{-1/3}\right]$. Flow of water out of overland flow

200   simulation domain only occurs horizontally at an outlet which is controlled by specifying a type

201   of boundary condition at the edge of the simulation domain. In a natural system, the outlet is

202   usually taken as the region where a river enters another water body such as stream or a lake. The

203   shallow overland flow formulation (equation 9) assumes that the flow depth is averaged-vertically

204   and neglects a vertical change in momentum in the column of surface water. To account for vertical

205   flow (into the subsurface from the surface), a formulation that couples the system of equations

206   through a boundary condition at the land surface becomes necessary. Equation (5) can be modified

207   to include an exchange rate with the subsurface, q_e, as:

208
$$\frac{\partial \psi_s}{\partial t} = \nabla \cdot (\vec{v} \psi_s) + q_s + q_e \qquad (9)$$

209 which is common in other IHMs. In ParFlow, the overland flow equations are coupled directly to

210 Richards' equation at the top boundary cell under saturated conditions. Conditions of continuity

211 of pressure (i.e. the pressures of the subsurface and surface domains are equal right at the ground

212 surface) and flux at the top cell of the boundary between the subsurface and surface systems are

213 assigned (Figure. 1). This assignment is done by setting pressure–head, in equation (1) equal to

214 the vertically–averaged surface pressure, ψ_s;

215
$$p = \psi_s = \psi, \qquad (10)$$

216 and the flux, q_e equal to the specified boundary conditions (e.g. Neumann or Dirichlet type). For

217 example, if Neumann type boundary conditions are specified, which are given as;

218
$$q_{BC} = -k_s k_r \nabla(\psi - z) \qquad (11)$$

219 and one solves for the flux term in equation (10), the result is;

220
$$q_e = \frac{\partial \|\psi, 0\|}{\partial t} - \nabla \vec{v} \|\psi, 0\| - q_s \qquad (12)$$

221 where the $\|\psi, 0\|$ operator is defined as the greater of the quantities, ψ and 0. Substituting equation

222 (12) for the boundary condition in equation (11), requiring the aforementioned flux continuity

223 $q_{BC} = q_e$, leads to

224
$$-k_s k_r \nabla(\psi - z) = \frac{\partial \|\psi, 0\|}{\partial t} - \nabla \cdot (\vec{v} \|\psi, 0\|) - q_s \qquad (13)$$

225 Equation (13) shows that the surface water equations are represented as a boundary condition to

226 the Richards' equation. That is, the boundary condition links flow processes in the subsurface with

227 those at the land surface. This boundary condition eliminates the exchange flux and accounts for

228   the movement of the free surface of ponded water at the land surface (Kollet and Maxwell, 2006;

229   Williams and Maxwell, 2011).

230   Many IHMs couple subsurface and surface flows making use of the exchange flux, q_e

231   model. The exchange flux between the domains (the surface and the subsurface) depends on

232   hydraulic conductivity and the gradient across some interface where indirect coupling is used

233   (VanderKwaak, 1999; Panday and Huyakorn, 2004). The exchange flux concept gives a general

234   formulation of a single set of coupled surface-subsurface equations. The exchange flux term, q_e

235   may be included in the shallow overland flow continuity equation as the exchange rate term with

236   the subsurface (equation 9) in a coupled system (Kollet and Maxwell, 2006).

237   Figure. 1 Caption: Coupled surface and subsurface flow systems. Note in this figure the physical

238   system is represented on the left and a schematic of the overland flow boundary condition

239   (continuity of pressure and flux at the ground surface) is on the right. The equation, $p = \psi_s = \psi$

240   in Figure. 1 signifies that the vertically averaged surface pressure and subsurface pressure head are

241   equal right at the land surface.

242

243   2.4 Multi-Phase Flow and Transport Equations

244   Most applications of the code have reflected ParFlow's core functionality as a single-phase

245   flow solver, but there are also embedded capabilities for multi-phase flow of immiscible fluids and

246   solute transport. Multi–phase systems are distinguished from single–phase systems by the presence

247   of one or more interfaces separating the phases, with moving boundaries between phases. The flow

248 equations that are solved in multi–phase systems in a porous medium comprise a set of mass

249 balance and momentum equations. The equations are given by:

250
$$\frac{\partial}{\partial t}(\phi \rho_i S_i) + \nabla.(\phi \rho_i S_i \vec{v}_i) - \rho_i Q_i = 0, \qquad (14)$$

251
$$\phi S_i \vec{v}_i + \lambda_i.(\nabla p_i - \rho_i \vec{g}) = 0, \qquad (15)$$

252 where $i = 1, \dots, n$ denotes a given phase (such as air or water). In these equations, ϕ is the intrinsic

253 medium porosity $[-]$ which explains the fluid capacity of the porous medium, and for each phase,

254 i, $S_i(x,t)$ is the saturation $[-]$ which indicates the content of phase i in the porous medium, $\vec{v}_i(x,t)$

255 represent Darcy velocity vector $[\text{LT}^{-1}]$, $Q_i(x,t)$ stands for source/sink term $[\text{T}^{-1}]$, $p_i(x,t)$ is the

256 average pressure $[\text{ML}^{-1}\text{T}^{-2}]$, $\rho_i(x,t)$ is the mass density $[\text{ML}^{-3}]$, λ_i is the mobility $[\text{L}^3\text{TM}^{-1}]$, $\vec{g}$

257 is the gravity vector $[\text{LT}^{-2}]$, and t is the time. ParFlow solves for the pressures on a discrete mesh

258 and uses a time-stepping algorithm based on a mass conservative backward Euler scheme and

259 spatial discretization (a finite volume method). ParFlow's multi–phase flow capability has not been

260 applied in major studies, however, this capability is also available for testing (Ashby et al., 1993;

261 Tompson et al., 1994; Falgout et al., 1999; Maxwell et al., 2016).

262 The transport equations included in the ParFlow package describe mass conservation in a

263 convective flow (no diffusion) with degradation effects and adsorption included along with

264 extraction and injection wells (Beisman et al., 2015; Maxwell et al., 2016). The transport equation

265 is defined as follows:

266
$$\left(\frac{\partial}{\partial t}(\phi c_{i,j}) + \lambda_j \phi c_{i,j}\right) + \nabla.\left(c_{i,j}\vec{v}\right) = -\left(\frac{\partial}{\partial t}\left((1-\phi)\rho_s F_{i,j}\right) + \lambda_i (1-\phi)\rho_s F_{i,j}\right) +$$

267
$$\sum_k^{nI} \gamma_k^{I;i} \chi\Omega_k^I \left(c_{i,j} - c_{i,j}^{-k}\right) - \sum_k^{nE} \gamma_k^{E;i} \chi\Omega_k^E c_{i,j} \qquad (16)$$

268 where ϕ denotes the porosity of the flow medium $[-]$, $c_{i,j}(x,t)$ represents concentration fraction

269 of contaminant $[-]$, $\vec{v}(x,t)$ is the Darcy velocity vector $[\mathrm{LT}^{-1}]$, λ_i is degradation rate $[\mathrm{T}^{-1}]$,

270 $F_i(x,t)$ is the mass concentration $[\mathrm{L}^3\mathrm{M}^{-1}]$, $\rho_s(x)$ is the density of the solid mass $[ML^{-3}]$, n_I is

271 injection wells $[-]$, $\gamma_k^{I;i}(t)$ is injection rate $[\mathrm{T}^{-1}]$, $\Omega_k^I(x)$ represent the area of the injection well

272 $[-]$, $c_{i,j}^{-k}(x,t)$ is the injected concentration fraction $[-]$, n_E is the extraction wells $[-]$, $\gamma_k^{E;i}(t)$ is

273 extraction rate $[\mathrm{T}^{-1}]$, $\Omega_k^E(x)$ is an extraction well area $[-]$, $i = 0, \ldots, n_{p-1}$ $(n_p \in \{1,2,3\})$ is the

274 number of phases, $j = 0, \ldots, n_c - 1$ represents the number of contaminants, $c_{i,j}$ is the

275 concentration of contaminant j in phase i, k is hydraulic conductivity $[\mathrm{LT}^{-1}]$, $\chi\Omega_k^I$ is the

276 characteristic function of an injection well region, and $\chi\Omega_k^E$ is the characteristic function of an

277 extraction well region. The mass concentration term, $F_{i,j}$ is taken to be instantaneous in time and

278 a linear function of contaminant concentration:

279 $$F_{i,j} = K_{d;j} c_{i,j} \tag{17}$$

280 where $K_{d;j}$ is the distribution coefficient of the component $[\mathrm{L}^3\mathrm{M}^{-1}]$. The transport/advection

281 equation or convective flow calculation performed by ParFlow offers a choice of a first-order

282 explicit upwind scheme or a second-order explicit Godunov scheme. The advection calculations

283 are discretized as boundary value problems for each primary dimension over each compute cell.

284 The discretization is a fully-explicit, forward Euler first-order accurate in time approach. The

285 implementation of a second-order explicit Godunov scheme (second-order advection scheme)

286 minimizes numerical dispersion and presents accurate computational process at these time scales

287 than either an implicit or lower-order explicit scheme. Stability issue here is that the simulation

288   timestep is restricted via the courant-Friedrichs-Lewy (CFL) condition, which demands that time

289   steps are chosen small enough to ensure that mass not be transported more than one grid cell in a

290   single timestep in order to maintain stability (Beisman, 2007).

291

292   2.5 Computational Grids

293   An accurate numerical approximation of a set of partial differential equations is strongly

294   dependent on the simulation grid. Integrated hydrologic models can use unstructured or structured

295   meshes for the discretization of the governing equations. The choice of grid type to adopt is

296   problem-specific and often a subjective choice since the same domain can be represented in many

297   ways, but there are some clear tradeoffs. For example, structured grid models, such as ParFlow,

298   may be preferred to unstructured grid models because structured grids provide significant

299   advantages in computational simplicity and speed, and are amenable to efficient parallelization

300   (Durbin, 2002; Kumar et al., 2009; Osei-Kuffuor et al., 2014). ParFlow adopts a regular, structured

301   grid specifically for its parallel performance. There are currently two regular grid formulations

302   included in ParFlow, an orthogonal grid and a terrain-following formulation (TFG); both allow for

303   variable vertical discretization (thickness over an entire layer) over the domain.

304   2.5.1 Orthogonal Grid

305   Orthogonal grids have many advantages, and many approaches are available to transform

306   an irregular grid into an orthogonal grid such as conformal mapping. This mapping defines a

307   transformed set of partial differential equations using an elliptical system with "control functions"

308   determined in such a way that the generated grid would be either orthogonal or nearly orthogonal.

309   However, conformal mapping may not allow flexibility in the control of the grid node distribution,

310   which diminishes its usefulness with complex geometries (Mobley and Stewart, 1980; Haussling

311   and Coleman, 1981; Visbal and Knight, 1982; Ryskin and Leal, 1983; Allievi and Calisal, 1992;

312   Eca, 1996).

313   A Cartesian, regular, orthogonal grid formulation is implemented by default in ParFlow,

314   though some adaptive meshing capabilities are still included in the source code. For example,

315   layers within a simulation domain can be made to have varying thickness. The upper portion of

316   Figure 2 shows the standard way topography or any other non-rectangular domain boundaries are

317   represented in ParFlow. The domain limits, and any other internal boundaries, can be defined using

318   grid-independent triangulated irregular network (TIN) files that define a geometry, or a gridded

319   indicator file can be used to define geometric elements. ParFlow uses octree space partitioning

320   algorithm (a grid-based algorithm or mesh generators filled with structured grids) (Maxwell, 2013)

321   to depict complex structures/land surface representations (e.g. topography, watershed boundaries,

322   and different hydrologic facies) in three-dimensional space (Kollet et al., 2010). These land surface

323   features are mapped onto the orthogonal grid, and looping structures that encompass these irregular

324   shapes are constructed (Ashby et al., 1997). The grid cells above ground surface are inactive

325   (shown in upper region of Figure 2) and are stored in the solution vector but not included in the

326   solution.

327   2.5.2 Terrain Following Grid

328   The inactive portion of a watershed defined with an orthogonal grid can be quite large in

329   complex watersheds with high-relief. In these cases, it is advantageous to use a grid that allows

16

330 these regions to be omitted. ParFlow's structured grid conforms to the topography via

331 transformation by the terrain following grid formulation. This transform alters the form of Darcy's

332 law to incorporate a topographic slope component. For example, subsurface fluxes are computed

333 separately in both x and y directions making use of the terrain following grid transform as:

334 $$q_x = K\sin(\theta_x) + K\frac{\partial p}{\partial y}\cos(\theta_x), \text{ and}$$

335 $$q_y = K\sin(\theta_y) + K\frac{\partial p}{\partial y}\cos(\theta_y) \qquad (18)$$

336 where q_x and q_y represent source/sink terms, such as fluxes, that include potential recharge flux

337 at the ground surface $[\text{LT}^{-1}]$, p is the pressure head $[\text{L}]$; K is the saturated hydraulic conductivity

338 tensor , $[\text{LT}^{-1}]$, θ is the local angle $[-]$ of topographic slope, S_x and S_y in the x and y directions

339 and may be presented as $\theta_x = \tan^{-1} S_x$ and $\theta_y = \tan^{-1} S_y$ respectively (Weill et al., 2009). The

340 terrain following grid formulation comes handy when solving coupled surface and subsurface

341 flows (Maxwell, 2013). The terrain following grid formulation uses the same surface slopes

342 specified for overland flow to transform the grid, whereas the slopes specified in the orthogonal

343 grid are only used for 2-D overland flow routing and do not impact the subsurface formulation

344 (see Figure 2). Note that TIN files can still be used to deactivate portions of the transformed

345 domain.

346

347 Figure 2 Caption: Representation of orthogonal (upper) and the terrain following (lower) grid

348 formulations and schematics of the related finite difference dependences (left). The i, j, and k are

349 the x, y, and z cell indices

350

351   3.   Equation Discretization and Solvers

352   The core of the ParFlow code is its library of numerical solvers. As noted above, in most

353   cases, the temporal discretization of the governing equations uses an implicit (backward Euler)

354   scheme; with cell-centered finite differences in spatial dimensions. Different components of this

355   solution framework have been developed for the various operational modes of ParFlow including

356   an inexact Newton-Krylov nonlinear solver (section 3.1), a multigrid algorithm (section 3.2), and

357   a multigrid-preconditioned conjugate gradient (MGCG) solver in (section 3.3). The conditions,

358   requirements, and constraints on the solvers depend on the specifics of the problem being solved,

359   and some solvers tend to be more efficient (faster overall convergence) than others for a given

360   problem. The core structure of these solvers and some of their implementation details are given

361   below, with an emphasis on the main concepts behind each solver.

362

363   3.1 Newton–Krylov solver for Variably Saturated Flow

364   The cell-centered fully-implicit discretization scheme applied to Richards' equation leads

365   to a set of coupled discrete nonlinear equations that need to be solved at each time step, and, for

366   variably saturated subsurface flow, ParFlow does this with the inexact Newton-Krylov method

367   implemented in the KINSOL package (Hindmarsh et al., 2005; Collier et al., 2015). Newton-

368   Krylov methods were initially utilized in the context of partial differential equations by (Brown

369   and Saad, 1990). In the approach, coupled nonlinear system as a result of discretization of the

370   partial differential equation is solved iteratively. Within each iteration, the nonlinear system is

371   linearized via a Taylor expansion. After linearization, an iterative Krylov method is used to solve

372   the resulting linear Jacobian system (Woodward, 1998; Osei-Kuffuor et al., 2014). For variably

373   saturated subsurface flow, ParFlow uses the GMRES Krylov method (Saad and Schultz, 1986).

374   Figure 3 is a flow chart of the solution technique ParFlow uses to provide approximate solutions

375   to systems of nonlinear equations.

376

377   Figure 3 caption: Working flow chart of ParFlow's solver for linear and non-linear system solution

378

379   The benefit of this Newton-Krylov method is that the Krylov linear solver requires only

380   matrix-vector products. Because the system matrix is the Jacobian of the nonlinear function, these

381   matrix-vector products may be approximated by taking directional derivatives of the nonlinear

382   function in the direction of the vector to be multiplied. This approximation is the main advantage

383   of the Newton-Krylov approach as it removes the requirement for matrix entries in the linear

384   solver. An inexact Newton method is derived from a Newton method by using an approximate

385   linear solver at each nonlinear iteration, as is done in the Newton-Krylov method (Dembo et al.,

386   1982; Dennis and Schabel, 1996). This approach takes advantage of the fact that when the

387   nonlinear system is far from converged, the linear model used to update the solution is a poor

388   approximation. Thus, the convergence criteria of early linear system solve is relaxed. The tolerance

389   required for solution of the linear system is decreased as the nonlinear function residuals approach

390   zero. The convergence rate of the resulting nonlinear solver can be linear or quadratic, depending

391   on the algorithm used. Through the KINSOL package, ParFlow can either use a constant tolerance

392 factor or ones from (Eisenstat and Walker, 1996). Krylov methods can be very robust, but they

393 can be slow to converge. As a result, it is often necessary to implement a preconditioner, or

394 accelerator, for these solvers.

395

396   3.2 Multigrid Solver

397   Multigrid (MG) methods constitute a class of techniques or algorithms for solving

398 differential equations (system of equations) using a hierarchy of discretization (Volker, 1987;

399 Briggs et al., 2000). Multigrid algorithms are applied primarily to solve linear and nonlinear

400 boundary value problems and can be used as either preconditioners or solvers. The most efficient

401 method for preconditioning the linear systems in ParFlow is the ParFlow Multigrid algorithm

402 (PFMG) (Ashby and Falgout, 1996; Jones and Woodward, 2001). Multigrid algorithms arise from

403 discretization of elliptic partial differential equations (Briggs et al., 2000), and, in ideal cases, have

404 convergence rates that do not depend on the problem size. In these cases, the number of iterations

405 remains constant even as problems sizes grow large. Thus, the algorithm is algorithmically

406 scalable. However, it may take longer to evaluate each iteration as problem sizes increase. As a

407 result, ParFlow utilizes the highly efficient implementation of PFMG in the hypre library (Falgout

408 and Yang, 2002).

409   For variably saturated subsurface flow, ParFlow uses the Newton-Krylov method coupled

410 with a multigrid preconditioner to accurately solve for the water pressure (hydraulic head) in the

411 subsurface and diagnoses the saturation field (which is used in determining the water table).

412 (Woodward, 1998; Jones and Woodward, 2000, 2001; Kollet et al., 2010). The water table is

413   calculated for computational cells having hydraulic heads above the bottom of the cells. Generally,

414   a cell is saturated if the hydraulic head in the cell is above the node elevation (cell center) or the

415   cell is unsaturated if the hydraulic head in the cell is below the node elevation. For saturated flow,

416   ParFlow uses the conjugate gradient method also coupled with a multigrid method. It is important

417   to note that subsurface flow systems are usually much larger radially than they are thick, so it is

418   common for the computational grids to have highly anisotropic cell aspect ratios to balance the

419   lateral and vertical discretization. Combined with anisotropy in the permeability field, these high

420   aspect ratios produce numerical anisotropy in the problem, which can cause the multigrid

421   algorithms to converge slowly (Jones and Woodward, 2001). To correct this problem, a

422   semicoarsening strategy or algorithm is employed, where the grid is coarsened in one direction at

423   a time. The direction chosen is the one with the smallest grid spacing i.e. the tightest coupling. In

424   an instance where more than one direction has the same minimum spacing, then the algorithm

425   chooses the direction in the order of x, followed by y, and then in z. To decide on how and when

426   to terminate the coarsening algorithm, Ashby and Falgout (1996) determined that a

427   semicoarsening down to a $(1 \times 1 \times 1)$ grid is ideal for groundwater problems.

428

429   3.3 Multigrid-Preconditioned Conjugate Gradient (MGCG)

430   ParFlow uses the multigrid-preconditioned conjugate gradient (CG) solver to solve the

431   groundwater equations under steady-state, and fully saturated flow conditions (Ashby and Falgout,

432   1996). These problems are symmetric and positive definite, two properties for which the CG

433   method was designed to target. While CG lends itself to efficient implementations, the number of

434   iterations required to solve a system such as results from discretization of the saturated flow

435   equation increases as the problem size grows. The PFMG multigrid algorithm is used as a

436   preconditioner to combat this growth and results in an algorithm for which the number of iterations

437   required to solve the system grows only minimally. See Ashby and Falgout (1996) for a detailed

438   description of these solvers and the parallel implementation of the multigrid preconditioned CG

439   method in ParFlow (Gasper et al., 2014; Osei-Kuffuor et al., 2014).

440

441   3.4 Preconditioned Newton-Krylov for Coupled Subsurface – Surface Flows

442   As discussed above, in ParFlow the coupling between the subsurface and surface

443   flows is handled implicitly. ParFlow solves this implicit system with the inexact Newton-Krylov

444   method described above. However, in this case, the preconditioning matrix is adjusted to include

445   terms from the surface coupling. In the standard saturated or variably saturated case, the multigrid

446   method is given the linear system matrix, or a symmetric version, resulting from discretization of

447   the subsurface model. Because ParFlow uses a structured mesh, these matrices have a defined

448   structure making their evaluation and application of multigrid straightforward. Due to varying

449   topographic height of the surface boundary, where the surface coupling is enforced, the surface

450   effects add non-structured entries in the linear system matrices. These entries increase complexity

451   of the matrix entry evaluations and reduce effectiveness of the multigrid preconditioner. In this

452   case, the matrix-vector products are most effectively performed through computation of the linear

453   system entries, rather than the finite difference approximation to the directional derivative. For

454   the preconditioning, surface couplings are only included if they model flow between cells at the

22

455   same vertical height. This restriction maintains the structured property of the preconditioning

456   matrix while still including much of the surface coupling in the preconditioner. Both these

457   adjustments led to considerable speedup in coupled simulations (Osei-Kuffuor et al., 2014).

458

459   4. Parallel Performance Efficiency

460   Scaling efficiency metrics offer a quantitative method for evaluating the performance of

461   any parallel model. Good scaling generally means that the efficiency of the code is maintained as

462   the solution of the system of equations is distributed onto more processors or as the problem

463   resolution is refined and processing resources are added. Scalability can depend on the problem

464   size, the processor number, the computing environment, and the inherent capabilities of the

465   computational platform used e.g. choice of a solver. The performance of ParFlow (or any parallel

466   code) is typically determined through weak and strong scaling (Gustafson, 1988). Weak scaling

467   involves the measurement of code's efficiency in solving problems of increasing size (i.e.

468   describes how the solution time change with change in the number of processors for a fixed

469   problem size per processor). In weak scaling, the simulation time should remain constant, as the

470   size of the problem and number of processing elements grow such that the same amount of work

471   is conducted on each processing element. Following Gustafson (1988), scaled parallel efficiency

472   is given by:

473     $$E(n,p) = \frac{T(n,1)}{T(pn,p)} \qquad\qquad (19)$$

474   where $E(n,p)$ denotes parallel efficiency, T represents the run time as a function of the problem

475   size n, which is spread across several processors p. Parallel code is said to be perfectly efficient if

476    $E(n,p) = 1$, and the efficiency decreases as $E(n,p)$ approaches 0. Generally, parallel efficiency

477   decreases with increasing processor number as communication overhead between

478   nodes/processors becomes the limiting factor.

479   Strong scaling describes the measurement of how much the simulation or solution time

480   changes with the number of processors for a given problem of fixed total size (Amdahl, 1967). In

481   strong scaling, a fixed size task is solved on a growing number of processors, and the associated

482   time needed for the model to compute the solution is determined (Woodward, 1998; Jones and

483   Woodward). If the computational time decreases linearly with the processor number, a perfect

484   parallel efficiency, ($E = 1$) results. The value of E is determined using equation (19). ParFlow has

485   been shown to have excellent parallel performance efficiency, even for large problem sizes and

486   processor counts (see Table 1) (Ashby and Falgout, 1996; Kollet and Maxwell, 2006). Maxwell

487   (2013) examined the relative performance of preconditioning the variably saturated flow system

488   with the symmetric portion or full matrix for the system. Both options use ParFlow's multigrid

489   preconditioner. Solver performance was demonstrated by combining the analytical Jacobian and

490   the non-symmetric preconditioner.   The study showed that the non-symmetric linear

491   preconditioner presents efficient gains. A section of the study results is reproduced in Table 1, in

492   addition to other scaling studies demonstrating ParFlow's parallel efficiency. This tradeoff was

493   also examined in Jones and Woodward (2000).

494

495   Table 1: Details for the various parallel scaling studies conducted using ParFlow.

496

5. Coupling

Different integrated models including atmospheric or weather prediction models (e.g. Weather Research Forecasting Model, Advanced Regional Prediction System, Consortium for Small-Scale Modeling), land surface models (e.g. Common Land Model, Noah Land Surface Model), and a subsurface model (e.g. CruchFlow) have been coupled with ParFlow to simulate a variety of coupled earth system effects (see Figure 4(a)). Coupling between ParFlow and other integrated models was performed to better understand the physical processes that occur at the interfaces between the deeper subsurface and ground surface, and between the ground surface and the atmosphere. None of the individual models can achieve this on their own because ParFlow cannot account for land surface processes (e.g. evaporation), and atmospheric and land surface models generally do not simulate deeper subsurface flows (Ren and Xue, 2004; Chow et al., 2006; Beisman, 2007; Maxwell et al., 2007; Shi et al., 2014). Model coupling can be achieved either via "offline coupling" where models involved in the coupling process are run sequentially and interactions between them is one–way (i.e. information is only transmitted from one model to the other) or "online" where they interact and feedback mechanisms among components are represented (Meehl et al., 2005; Valcke et al., 2009). Each of the coupled models uses its own solver for the physical system it is solving, then information is passed between the models. As

514 long as each model exhibits good parallel performance, this approach still allows for simulations

515 at very high resolution, with a large number of processes (Beven, 2004; Ferguson and Maxwell,

516 2010; Shen and Phanikumar, 2010; Shi et al., 2014). This section focuses on the major couplings

517 between ParFlow and other codes. We point out specific functions of the individual models as

518 stand–alone codes that are relevant to the coupling process. In addition, information about the role

519 or contribution of each model at the coupling interface (see Figure 4(b)) that connects with

520 ParFlow are presented (Figure 5 shows the communication network of the coupled models). We

521 discuss couplings between ParFlow and its land surface model (a modified version of the original

522 Common Land Model introduced by Dai et al., (2003)), Consortium for Small-Scale Modeling

523 (COSMO), Weather Research Forecasting Model, Advanced Regional Prediction System, and

524 CruchFlow in sections 5.1, 5.2, 5.3, 5.4, and 5.5 respectively.

525 Figure 4(a) Caption: A pictorial description of the relevant physical environmental features and

526 model coupling. CLM represents the Community Land Model, a stand-alone Land Surface Model

527 (LSM) via which ParFlow couples' COSMO. The modified version of CLM by Dai et al., (2003)

528 and is not shown in Figure 4(a) because it is a module only for ParFlow, not really a stand-alone

529 LSM any longer.

530

531 Figure 4(b) Caption: Schematic showing information transmission at the coupling interface. PF,

532 LSM, and ATM indicate the portions of the physical system simulated by ParFlow, Land Surface

533 Models, and Atmospheric Models respectively. The downward and upward arrows indicate the

534   directions of information transmission between adjacent models. Note: Coupling between ParFlow

535   and CrunchFlow (not shown) occur within the subsurface.

536   5.1 ParFlow–Common Land Model (PF.CLM)

537   The Common Land Model (CLM) is a land surface model designed to complete land-

538   water-energy balance at the land surface (Dai et al., 2003). CLM parameterizes the moisture,

539   energy and momentum balances at the land surface and includes a variety of customizable land

540   surface characteristics and modules, including land surface type (land cover type, soil texture, and

541   soil color), vegetation and soil properties (e.g. canopy roughness, zero-plane displacement, leaf

542   dimension, rooting depths, specific heat capacity of dry soil, thermal conductivity of dry soil,

543   porosity), optical properties (e.g. albedos of thick canopy), and physiological properties related to

544   the functioning of the photosynthesis-conductance model (e.g. green leaf area, dead leaf, and stem

545   area indices). A combination of numerical schemes is employed to solve the governing equations.

546   CLM uses a time integration scheme which proceeds by a split-hybrid approach, where the solution

547   procedure is split into "energy balance" and "water balance" phases in a very modularized structure

548   (Mikkelson et al., 2013; Steiner et al., 2005, 2009). The CLM described here and as incorporated

549   in ParFlow is a modified version of the original CLM introduced by Dai et al., (2003). This results

550   in the coupled model, PF.CLM i.e. ParFlow with its own land surface model. The modified CLM

551   is composed of a series of land surface modules that are called as a subroutine within ParFlow to

552   compute energy and water fluxes (e.g. evaporation and transpiration) to and out of the soil. For

553   example, the modified CLM computes bare ground surface evaporative flux, E_{gr} as

554
$$E_{gr} = -\beta \rho_a u_* q_*$$ (20)

555   where β (dimensionless) denotes soil resistance factor, ρ_a represents air density $[ML^{-3}]$, u_*

556   represents friction velocity $[LT^{-1}]$, and q_* (dimensionless) stands for humidity scaling parameter

557   (Jefferson and Maxwell, 2015). Evapotranspiration for vegetated land surface, E_{veg} is computed

558   as

559
$$E_{veg} = \left[R_{pp,dry} + L_w\right] L_{SAI} \left[\frac{\rho_a}{r_b}\left(q_{sat} - q_{af}\right)\right]$$ (21)

560   where r_b is the air density boundary resistance factor $[LT^{-1}]$, q_{sat} (dimensionless) is saturated

561   humidity at the land surface, and q_{af} (dimensionless) is the canopy humidity. Combination of q_{sat}

562   and q_{af} forms the potential evapotranspiration. The potential evapotranspiration is divided into

563   transpiration $R_{pp,dry}$ (dimensionless) which depends on the dry fraction of the canopy, and

564   evaporation from foliage covered by water L_w (dimensionless). L_{SAI} (dimensionless) is summation

565   of the leaf and stem area indices which estimates the total surface from which evaporation can

566   occur. A detailed description of the equations CLM of PF.CLM uses can be found in Jefferson et

567   al., (2015), (2017), and Jefferson and Maxwell, (2015).

568   The coupled model PF.CLM simulates variably saturated subsurface flow, surface or

569   overland flow, and above-ground processes. PF.CLM was developed prior to the current

570   community land model (see section 5.2), and the module structure of the current and early versions

571   are different. PF.CLM has been updated over the years to improve its capabilities. PF.CLM was

572   first done in the early 2000's, as an undiversified, a column proof-of-concept model, where data

573   or message was transmitted between the coupled models via input/output files (Maxwell and

574   Miller, 2005). Later, PF.CLM was presented in a distributed or diversified approach with a parallel

575   input/output file structure where CLM is called as a set sequence of steps within ParFlow (Kollet

576   and Maxwell, 2008a). These modifications, for example, were done to incorporate subsurface

577   pressure values from ParFlow into chosen computations (Jefferson and Maxwell, 2015). Within

578   the coupled PF.CLM, ParFlow solves the governing equations for overland and subsurface flow

579   systems and the CLM modules add the energy balance and mass fluxes from the soil, canopy, and

580   root zone that can occur (i.e. interception, evapotranspiration etc.) (Maxwell and Miller, 2005).

581   At the coupling interface where the models overlap and communicate (see Figure 4(b)),

582   ParFlow calculates and passes soil moisture as well as pressure heads of the subsurface to CLM,

583   and CLM calculates and transmits transpiration from plants, canopy and ground surface

584   evaporation, snow accumulation and melt, and infiltration from precipitation to ParFlow (Ferguson

585   et al., 2016). In short, CLM does all canopy water balances and snow, but once the water through

586   falls to the ground, or snow melts, ParFlow takes over and estimates the water balances via the

587   nonlinear Richards' equation. The coupled model, PF.CLM, has been shown to more accurately

588   predict root-depth soil moisture compared to the uncoupled model. This increased accuracy results

589   from the coupling of soil saturations determined by ParFlow and their impacts on other processes

590   including runoff and infiltration (Kollet, 2009; Shrestha et al., 2014; Gebler et al., 2015; Gilbert

591   and Maxwell, 2016). For example, (Maxwell and Miller, 2005) found that simulations of deeper

592   soil saturation (more than 40cm) vary between PF.CLM and uncoupled models, with PF.CLM

593   simulations closely matching the observed data. Table 2 contains summaries of studies conducted

594 with ParFlow coupled to either the original version of CLM by (Dai et al., 2003) or modified CLM

595 (ParFlow land surface model).

596   5.1.1. ParFlowE–Common Land Model (ParFlowE[CLM])

597   It is well established that PF.CLM does perform well in estimating all canopy water and

598 subsurface water balances (Maxwell and Miller, 2005; Mikkelson et al., 2013; Ferguson et al.,

599 2016). ParFlow, as a component of the coupled model has been modified into a new parallel

600 numerical model, ParFlowE to incorporate the more complete heat equation coupled to variably

601 saturated flow. ParFlowE simulates coupling of terrestrial hydrologic and energy cycles i.e.

602 coupled moisture, heat, and vapor transport in the subsurface. ParFlowE is based on the original

603 version of ParFlow having identical solution schemes and coupling approach with CLM. A

604 coupled three-dimensional subsurface heat transport equation is implemented in ParFlowE using

605 a cell-centered finite difference scheme in space and an implicit backward Euler differencing

606 scheme in time. However, the solution algorithm employed in ParFlow is fully exploited in

607 ParFlowE where the solution vector of the Newton-Krylov method was extended to two

608 dimensions (Kollet et al., 2009). In some integrated and climate models, the convection term of

609 subsurface heat flux and the effect of soil moisture on energy transport is neglected due to

610 simplified parameterizations and computational limitations. However, both convection and

611 conduction terms are considered in ParFlowE (Khorsandi et al., 2014). In ParFlowE, functional

612 relationships (i.e. equations of state) are performed to relate density and viscosity to temperature

613 and pressure, and thermal conductivity to saturation. That is, modeling thermal flows by relating

614 these parameterizations in simulating heat flow is an essential component of ParFlowE. In

Geoscientific
Model Development
Discussions

615   coupling between ParFlowE and CLM, ParFlowE[CLM], the one-dimensional subsurface heat

616   transport in the CLM is replaced by the three-dimensional heat transport equation including the

617   process of convection of ParFlowE. CLM computes mass and energy balances at ground surface

618   that lead to moisture fluxes and pass these fluxes to the subsurface moisture algorithm of

619   ParFlowE[CLM]. These fluxes are used in computing subsurface moisture and temperature fields

620   which are then passed back to the CLM.

621

622   5.2 ParFlow in the Terrestrial Systems Modeling Platform, TerrSysMP

623   ParFlow is part of the Terrestrial System Modeling Platform TerrSysMP, which comprise

624   the nonhydrostatic fully compressible limited-area atmospheric prediction model, COSMO,

625   designed for both operational numerical weather prediction and various scientific applications on

626   the meso–β (horizontal scales of 20–200km) and meso–γ (horizontal scales of 2–20km) (Duniec

627   and Mazur, 2011; Levis and Jaeger, 2011; Bettems et al., 2015), and the Community Land Model

628   version 3.5 (CLM3.5). Currently, it is used in direct simulations of severe weather events triggered

629   by deep moist convection, including intense mesoscale convective complexes, prefrontal squall–

630   line storms, supercell thunderstorms, and heavy snowfall from wintertime mesocyclones. COSMO

631   solves nonhydrostatic, fully compressible hydro–thermodynamical equations in advection form

632   using the traditional finite difference method (Vogel et al., 2009; Mironov et al., 2010; Baldauf et

633   el., 2011; Wagner et al., 2016).

634   Coupling between ParFlow and the COSMO model is performed via CLM3.5 (Gasper et

635   al., 2014; Shrestha et al., 2014; Keune et al., 2016). Similar to the Common Land Model (by (Dai

636   et al., 2003)), CLM3.5 module accounts for surface moisture, carbon, and energy fluxes between

637   the shallow or near-surface soil (discretized/specified top soil layer), snow, and the atmosphere

638   (Oleson et al., 2008). The model components of a fully coupled system consisting of COSMO,

639   CLM3.5, and ParFlow are assembled by making use of the multiple–executable approach (e.g.

640   with OASIS3-MCT model coupler). The OASIS3-MCT coupler employs communication

641   strategies based on the message passing interface standards, MPI1/MPI2 and the Project for

642   Integrated Earth System Modeling, PRISM, Model Interface Library (PSMILe) for parallel

643   communication of two–dimensional arrays between OASIS3-MCT coupler and the coupling

644   models (Valcke et al., 2012; Valcke, 2013). The OASIS3-MCT specifies the series of coupling,

645   frequency of the couplings, the coupling fields, the spatial grid of the coupling fields,

646   transformation type of the (two–dimensional) coupled fields, and simulation time management and

647   integration.

648   At the coupling interface, the OASIS3-MCT interface interchanges the atmospheric

649   forcing terms and the surface fluxes in serial mode. The lowest level and current time step of the

650   atmospheric state of COSMO is used as the forcing term for CLM3.5. CLM3.5 then computes and

651   returns the surface energy and momentum fluxes, outgoing longwave radiation, and albedo to

652   COSMO (Baldauf et al., 2011). The air temperature, wind speed, specific humidity, convective

653   and grid-scale precipitation, pressure, incoming shortwave (direct and diffuse) and longwave

654   radiation, and measurement height are sent from COSMO to CLM3.5. In CLM3.5, a mosaic/tilling

655   approach may be used to represent the subgrid-scale variability of land surface characteristics,

656   which considers a certain number of patches/tiles within a grid cell. The surface fluxes and surface

657   state variables are first calculated for each tile and then spatially averaged over the whole grid cell

658   (Shrestha et al., 2014) . As with PF.CLM3.5, the one–dimensional soil column moisture predicted

659   by CLM3.5 gets replaced by ParFlow's variably saturated flow solver, so ParFlow is responsible

660   for all calculations relating soil moisture redistribution and groundwater flow.   Within the

661   OASIS3-MCT ParFlow sends the calculated pressure and relative saturation for the coupled region

662   soil layers to CLM3.5. The CLM3.5 also transmits depth-differentiated source and sink terms for

663   soil moisture including soil moisture flux e.g. precipitation, and soil evapotranspiration for the

664   coupled region soil layers to ParFlow. Applications of TerrSysMP in fully coupled mode from

665   saturated subsurface across the ground surface into the atmosphere include a study on the impact

666   of groundwater on the European heat wave 2003 and the influence of anthropogenic water use on

667   the robustness of the continental sink for atmospheric moisture content (Keune et al., 2016).

668   5.3 ParFlow–Weather Research Forecasting models (PF.WRF)

669   The Weather Research and Forecast (WRF) is a mesoscale numerical weather prediction

670   system designed to be flexible and efficient in a massively parallel computing architecture. WRF

671   is a widely used model that provides a common framework for idealized dynamical studies, full

672   physics numerical weather prediction, air-quality simulations, and regional climate simulations

673   (Michalakes et al., 1999, 2001; Skamarock et al., 2005). The model contains numerous mesoscale

674   physics options such as microphysics parameterizations (including explicitly resolved water vapor,

675   cloud, and precipitation processes), surface layer physics, shortwave radiation, longwave

676   radiation, land surface, planetary boundary layer, data assimilation, and other physics and

677   dynamics alternatives suitable for both large-eddy and global-scale simulations. Similar to

678   COSMO, the WRF model is a fully compressible, conservative-form, non-hydrostatic atmospheric

679   model which uses time-splitting integration techniques (discussed below) to efficiently integrate

680   the Euler equations (Skamarock and Klemp, 2007).

681   The ParFlow WRF coupling (PF.WRF) extends the WRF platform down to bedrock by

682   including highly resolved three-dimensional groundwater and variably saturated shallow or deep

683   vadose zone flows, and a fully integrated lateral flow above ground surface (Molders and Ruhaak,

684   2002; Seuffert et al., 2002; Anyah et al., 2008; Maxwell et al., 2011). The land surface model

685   portion that links ParFlow to WRF is supplied by WRF through its land surface component, the

686   Noah Land Surface Model (Ek et al., 2003); the standalone version of WRF has no explicit model

687   of subsurface flow. Energy and moisture fluxes from the land surface are transmitted between the

688   two models via the Noah LSM which accounts for the coupling interface, and which is

689   conceptually identical to the coupling in PF-COSMO. The three-dimensional variably saturated

690   subsurface and two-dimensional overland flow equations, and the three-dimensional atmospheric

691   equations given by ParFlow and WRF are simultaneously solved by the individual model solvers.

692   Land surface processes, such as evapotranspiration, are determined in the Noah LSM as a function

693   of potential evaporation and vegetation fraction. This effect is calculated with the formulation:

694              $$E(x) = F^{fx}(1 - f_{avg})E_{pot} \qquad (22)$$

695   where $E(x)$ stands for rate of soil evapotranspiration (length per unit time), fx represents empirical

696   coefficient, f_{avg} denotes vegetation fraction, and E_{pot} is potential evaporation, determined that

697   depends on atmospheric conditions from the WRF boundary layer parameterization (Ek et al.,

698   2003). The vegetation fraction is zero over bare soils (i.e. only soil evaporation), so equation 22

699   becomes:

700 $$E(x) = F^{fx}E_{pot} \qquad (23)$$

701   The quantity F is parameterized as follows:

702 $$F = \frac{\phi S_w - \phi S_{res}}{\phi - \phi S_{res}}, \qquad (24)$$

703   where ϕ is porosity, S_w and S_{res} are relative saturation and residual saturation respectively, from

704   vanGenuchten relationships (VanGenuchten, 1980; Williams and Maxwell, 2011). Basically, F

705   refers to the parameterization of the interrelationship between evaporation and near-ground soil

706   water content and provides one of the connections between Noah LSM and ParFlow, and thus

707   WRF.

708   In the presence of a vegetation layer, plant transpiration (length per unit time) is determined

709   as follows:

710 $$T(x,z) = G(z)C_{plant}f_{veg}E_{pot}, \qquad (25)$$

711   where $C_{plant}(-)$ represents a constant coefficient between 0 and 1, which depends on vegetation

712   species, and the $G(z)$ function represents soil moisture which provides other connection between

713   the coupled models (i.e. ParFlow, Noah, and WRF). The solution procedure of PF.WRF uses an

714   operator–splitting approach where both model components use the same time step. WRF soil

715   moisture information including runoff, surface ponding effects, unsaturated and saturated flow,

716   which includes an explicitly resolved water table are calculated and sent directly to the Noah LSM

717   within WRF by ParFlow and utilized by the Noah LSM in the next time step. WRF supplies

718   ParFlow with evapotranspiration rates and precipitation via the Noah LSM (Jiang et al., 2009).

719   The interdependence between energy and land balance of the subsurface, ground surface, and

720   lower atmosphere can fully be studied with this coupling approach. The coupled PF.WRF via the

721   Noah-LSM has been used to simulate explicit water storage and precipitation within basins, to

722   simulate surface runoffs and to simulate the land-atmosphere feedbacks and wind patterns as a

723   results of subsurface heterogeneity (Maxwell et al., 2011; Williams and Maxwell, 2011). Studies

724   with coupled model PF.WRF are highlighted in Table 2.

725   5.4 ParFlow–Advanced Regional Prediction System (PF. ARPS).

726   The Advanced Regional Prediction System (ARPS) composed of a parallel mesoscale

727   atmospheric model created to explicitly predict convective storms and weather systems. The ARPS

728   platform aids in effectively investigating the changes and predictability of storm-scale weather in

729   both idealized and more realistic settings. The model deals with the three dimensional, fully

730   compressible, non-hydrostatic, spatially filtered Navier-Stokes equations (Rihani et al., 2015). The

731   governing equations include conservation of momentum, mass, water, heat or thermodynamic,

732   turbulent kinetic energy, and the equation of state of moist air making use of a terrain-following

733   curvilinear coordinate system (Xue et al., 2000). The governing equations presented in a

734   coordinate system with z as the vertical coordinate are given as

735    $$\frac{dV}{dt} = -2\Omega \times V - \frac{1}{\rho}\nabla P + g + F \qquad (26)$$

736    $$\frac{d\rho}{dt} = -\rho\nabla.V \qquad (27)$$

737
$$\frac{dT}{dt} = -\frac{RT}{C_v} \, \nabla.V + \frac{Q}{C_v} \tag{28}$$

738
$$P = \rho RT \tag{29}$$

739 Equations (26) to (29) are momentum, continuity, thermodynamic and equation of state,

740 respectively. The material (total) derivative d/dt is defined as

741
$$\frac{d}{dt} = \frac{\partial}{\partial t} + \nabla.V \tag{30}$$

742 The variables V, ρ, T, P, g, F, Q in equations (26) to (29) represent velocity, density, temperature,

743 pressure, gravity, frictional force, and the diabatic heat source, respectively (Xu et al., 1991). The

744 ARPS model employs high-order monotonic advection technique for scalar transport and fourth-

745 order advection for other variables e.g. mass density and mass mixing ratio. A split-explicit time

746 advancement scheme is utilized with leapfrog on the large time steps, and an explicit and implicit

747 scheme for the smaller time steps is used to inculcate the acoustic terms in the equations (Rihani

748 et al., 2015).

749   The PF.ARPS forms a fully–coupled model that simulates spatial variations in above

750 ground processes and feedbacks, forced by physical processes in the atmosphere and the below the

751 ground surface. In the coupling process, ARPS land surface model forms the interface between

752 ParFlow and ARPS to transmit information (i.e. surface moisture fluxes) between the coupled

753 models. ParFlow as a component of the coupled model replaces the subsurface hydrology in the

754 ARPS land surface model. Thus, ARPS is integrated into ParFlow as a subroutine to create a

755 numerical overlay at the coupling interphase (specified layers of soil within the land surface model

756 in ARPS) with the same number of soil layers at the ground surface within ParFlow. The solution

757 approach employed is an operator-splitting that allows ParFlow to match the ARPS internal

758 timesteps. ParFlow calculates the subsurface moisture field at each timestep of a simulation and

759 passes the information to ARPS land surface model, which is used in each subsequent timestep.

760 At the beginning of each time step, the surface fluxes from ARPS that are important to ParFlow

761 include evapotranspiration rate and spatially–variable precipitation (Maxwell et al., 2007). PF.

762 ARPS has been applied to investigate the effects of soil moisture heterogeneity on atmospheric

763 boundary layer processes. PF.ARPS keeps a realistic soil moisture that is topographically-driven

764 distribution and shows spatiotemporal relationship between water depth, land surface and lower

765 atmospheric variables (Maxwell et al., 2007; Rihani et al., 2015). A summary of current studies

766 involving PF. ARPS is included in Table 2.

767

768   5.5 ParFlow–CrunchFlow (ParCrunchFlow)

769   CrunchFlow is a software package developed to simulate multicomponent multi-

770 dimensional reactive flow and transport in porous and/or fluid media (Steefel, 2009). Systems of

771 chemical reactions that can be solved by the code include kinetically controlled homogenous and

772 heterogeneous mineral dissolution reactions, equilibrium–controlled homogeneous reactions,

773 thermodynamically controlled reactions, and biologically–mediated reactions (Steefel and Lasaga,

774 1994; Steefel and Yabusaki, 2000). In CrunchFlow, discretization of the governing coupled partial

775 differential equations which connect subsurface kinetic reactions and multicomponent

776   equilibrium, flow and solute transport is based on finite volume. (Li et al., 2007; Li et al., 2010).

777   Coupling of reactions and transport in CrunchFlow that are available at runtimes are performed

778   using two approaches. These are briefly discussed below.

779   First, a global implicit or one–step method approach is based on a backwards Euler time

780   discretization, with a global solution of the coupled reactive transport equations using Newton's

781   method. This global implicit scheme solves the transport and reaction terms simultaneously (up to

782   two-dimensional) (Kirkner and Reeves, 1988; Steefel, 2009). Second, a time or operator splitting

783   of the reaction and transport terms which is based on an explicit forward Euler method; the

784   sequential non-iterative approach, SNIA (in which the transport and reaction terms are solved)

785   (Steefel and Van Cappellen, 1990; Navarre-Sitchler et al., 2011). The stability criteria associated

786   with the explicit approach is that the simulation timestep is restricted via the courant-Friedrichs-

787   Lewy (CFL) condition, under the circumstance that the transportation of mass does not occur over

788   multiple grid cell, but a single grid cell in a timestep. Thus, a small-time step must be used to

789   ensure this condition holds. This small step size may lead to simulations that will demand much

790   time to solve Beisman, (2007), so more processors are used, in order to decrease the processor

791   workload and decrease solution time of the simulation. Coupling of fully saturated flow to the

792   reactive transport calculations and coupling between a partially saturated flow and transport (flow

793   and diffusion) can be done successively. However, these simulations require calculations of the

794   flow and liquid saturation fields with a different model.

795   ParCrunchFlow is a parallel reactive transport model developed by combining ParFlow

796   with CrunchFlow. ParCrunchFlow relies on ParFlow's robustness ability to efficiently represent

797   heterogeneous domains and simulate complex flow to provide a more realistic representation of

798   the interactions between biogeochemical processes and non-uniform flow fields than the

799   uncoupled model. ParFlow provides solution of Richards' equation to ParCrunchFlow, which is

800   not present in the biogeochemical code CrunchFlow. ParCrunchFlow employs operator-splitting

801   method to reactive transport, in which the transport and reaction terms are decoupled and

802   calculated independently. Coupling between the models is achieved through a sequential non-

803   iterative approach, where the reaction terms in CrunchFlow's operator-splitting solver gets

804   connected to ParFlow's advection terms. A steady state governing differential equation for reaction

805   and advection (with no dispersion and diffusion terms) in a single-phase system is given by

806
$$\frac{\partial C_i}{\partial t} + \nabla . (V C_i) - R_i = 0 , \quad (i = 1, N_{tot}) \tag{31}$$

807   where C_i is the concentration of species i, V represents velocity of flow, R_i indicates total reaction

808   rate of species i, and N_{tot} represents total species number. In the coupling process, the advection

809   terms are calculated by ParFlow's transport solver through a first-order explicit upwind scheme or

810   a second-order explicit Godunov scheme. Low-order upwind weighting schemes can introduce

811   numerical dispersion, which can impact the simulated reactions, and a comparison of several

812   upwinding schemes can be found in (Benson et al., 2017). CrunchFlow calculates the reaction

813   terms using the Newton-Raphson method. For example, in the coupled–model ParCrunchFlow,

814   ParFlow code assigns all hydrological parameters, undertakes the functions relating to

815   parallelization including domain decomposition and message transmission, and solves for pressure

816   and flow fields. The CrunchFlow module is then used to evaluate all reaction terms and

817   conversions between mobile and immobile concentrations. Sequence of simulations of a floodplain

818   aquifer, comprising biologically mediated reduction of nitrate have been performed with

819   ParCrunchFlow. The simulations demonstrate that ParCrunchFlow realistically represents the

820   changes in chemical concentrations seen in most field scale systems than CrunchFlow alone

821   (summarized in Table 2) (Beisman, 2007; Beisman et al., 2015).

822   Figure 5 Caption: Schematic of the communication structure of the coupled models. Note: CLM

823   represents a stand-alone Community Land Model. The modified version of CLM by Dai et al.,

824   (2003) is not shown here because it is a module only for ParFlow, not really a stand-alone LSM

825   any longer.

826

827   6. Discussion and Summary

828   IHMs constitute classes of simulation tools ranging from simple lumped parameter models

829   to comprehensive deterministic, distributed and physically based modeling systems for simulation

830   of multiple hydrological processes (LaBolle et al., 2003; Castronova et al., 2013). They are

831   indispensable in studying the interactions between surface and subsurface systems. IHMs that

832   calculate surface and subsurface flow equations in a single matrix (Maxwell et al., 2015), scaling

833   from the beginning parts to the mouth of continental river basins at high-resolutions are essential

834   (Wood, 2009) in understanding and modeling surface-subsurface systems. IHMs have been used

835   to address surface and subsurface science and applied questions. For example, evaluating the

Geoscientific
Model Development
Discussions

836   effects of groundwater pumping on streamflow and groundwater resources (Markstrom et al.,

837   2008), evaluating relationship between topography and groundwater (Condon and Maxwell,

838   2015), coupling water flow and transport (Sudicky et al., 2008; Weill et al., 2011) and assessing

839   the resilience of water resources to human stressors or interventions and the variations in the

840   (Maxwell et al., 2015) over large spatial extents at high resolution. Modeling or simulation at large

841   spatial extents e.g. regional and continental scales and resolution e.g. $1km^2$ (see Figure 6) comes

842   with the associated computational load even on massively parallel computing architectures. IHMs,

843   such as ParFlow have overcome the computational burden of simulating or resolving questions

844   (e.g. involving approximating variably saturated and overland flow equations) beyond such levels

845   of higher spatial scales and resolutions. This capability may not be associated with more

846   conceptually based models which, for example, may not simulate lateral groundwater flow or

847   resolve surface and subsurface flow by specifying zones of groundwater network of stream before

848   performing a simulation (Maxwell et al., 2015).

849   Figure 6 Caption: Map of water table depth (m) over the simulation domain with two insets

850   zooming into the North and South Platte River basin, headwaters to the Mississippi River. Colors

851   represent depth in log scale (from 0.01 to 100 m) (Maxwell et al., 2015).

852   Figure 7 Caption: Map of hydraulic conductivity (K) and stream depth in the East Inlet watershed

853   in Colorado (Engdahl and Maxwell, 2015). This domain covers $30km^2$ using 3.1 million $20m^2$

854   (lateral grid cells. The springs emanating from within the hillslopes highlight the realism afforded

855   by integrated modeling at small scales.

856

857   ParFlow is based on efficient parallelism (high performance efficiency) and robust

858   hydrologic capabilities. The model solvers and numerical methods used are powerful, fast, robust,

859   and stable, which has contributed to the code's excellent parallel efficiency. As stated earlier,

860   ParFlow is very capable of simulating flows under saturated and variably saturated conditions i.e.

861   surface, vadose, and groundwater flows, even in highly heterogeneous environments. For example,

862   in simulation of surface flows (i.e. solving the kinematic wave overland flow equations), ParFlow

863   possess the ability to accurately solve streamflow (channelized flow) by using parameterized river

864   routing subroutines (Maxwell and Miller, 2005; Maxwell et al., 2007, 2011). ParFlow includes

865   coupling capabilities with a flexible coupling interface which has been utilized extensively in

866   resolving many hydrologic problems. The interface-based and process-level coupling used by

867   ParFlow is an example for enabling high-resolution, realistic modeling. However, based on the

868   applications, it would be worthwhile to create one, or several, generic coupling interfaces within

869   ParFlow to make it easier to use its surface/subsurface capabilities in other simulations.

870   Nonetheless, ParFlow has been used in coupling studies in simulating different processes and/or

871   systems including simulating energy and water budgets of the surface and subsurface (Rihani et

872   al., 2010; Mikkelson et al., 2013), surface water and groundwater flows and transport (Kollet and

873   Maxwell, 2006; Beisman, 2007; Beisman et al., 2015; Maxwell et al., 2015), and subsurface,

874   surface, and atmospheric mass and energy balance (Maxwell and Miller, 2005; Maxwell et al.,

875   2011; Shrestha et al., 2014; Sulis et al., 2017). Undoubtedly, such coupled-model simulations come

876   with computational burden and ParFlow performs well in overcoming such problems, even at high

877 spatial scale and resolutions. This capability of ParFlow (coupling with other models) is

878 continuously being exploited by hydrologic modelers, and new couplings are consistently being

879 established. For example, via model coupling, the entire transpiration process could be investigated

880 i.e. from carbon dioxide sequestration from the atmosphere by plants, subsurface moisture

881 dynamics and impacts, to oxygen production by plants. Likewise, land cover change effects on

882 mountain pine beetles may be investigated via coupling of integrated models. But these projected

883 research advances can only be achieved if the scientific community keeps advancing code

884 performance by developing, revising, updating, and rigorously testing these models' capabilities.

885 Presently, ParFlow's open source model and open developer community is fully

886 transparent, and this openness is a major difference between it and other models that has enabled

887 ParFlow to continue evolving. The user community is growing daily across the globe. Code

888 developers have made available, aside from the ParFlow working manual, an active and

889 frequently-updated blog (current blog: "http://parflow.blogspot.com/") and other sources

890 including "https://www.parflow.org" and "https://github.com/parflow" where code developers and

891 experienced users provide great information and suggestions that help in fixing bugs and ease

892 frustrations of other users. Over the years, these easily accessible resources have proven to be

893 helpful. The code is constantly updated through release of new versions with modifications

894 designed to meet varying hydrologic challenges and directions for applications across different

895 scales and fields. Further, there is a software development and sustainability plan to improve the

896 capabilities of ParFlow. ParFlow works very well on different computing architectures and

897 operating systems from "Laptops to Supercomputers" (single CPU, Linux clusters, highly scalable

898   systems including IBM Blue Gene) with the same source code and input on all platforms. The code

899   can use significant computational power and runs efficiently on supercomputing environments

900   (e.g. Edison, Cori, JUQUEEN, and Yellowstone). Through ParFlow hydrologic modelers have

901   available a very efficient yet still growing integrated hydrologic model to simulate and understand

902   surface-subsurface flows.

903   Code availability

904   ParFlow is an open–source, object–oriented, parallel watershed flow model developed by
905   community of scientists from the Environmental Protection Department at the Lawrence
906   Livermore National Laboratory (LLNL), Colorado School of Mines and F-Z Jülich with
907   supporting scientists from several other institutions. Versions of ParFlow are archived with
908   detailed   document   or   information   located   at:
909   http://inside.mines.edu/~rmaxwell/maxwell_software.shtml or obtain from commercially hosted
910   free SVN repository. Source code for the current ParFlow release "v3.5.0" can be downloaded at:
911   https://github.com/parflow/parflow/releases/tag/v3.5.0.

912   Author Contribution

913   Section 3 of the manuscript was written by Carol S. Woodward. Benjamin N. O. Kuffour and
914   Nicholas B. Engdahl wrote the other Sections, and the entire manuscript was edited by Laura E.
915   Condon, Stefan Kollet, and Reed M. Maxwell.

916   Competing Interest

917   We declare that no conflict of interest exist whatsoever between any of the authors and the editors
918   or the referees.

919   Acknowledgement
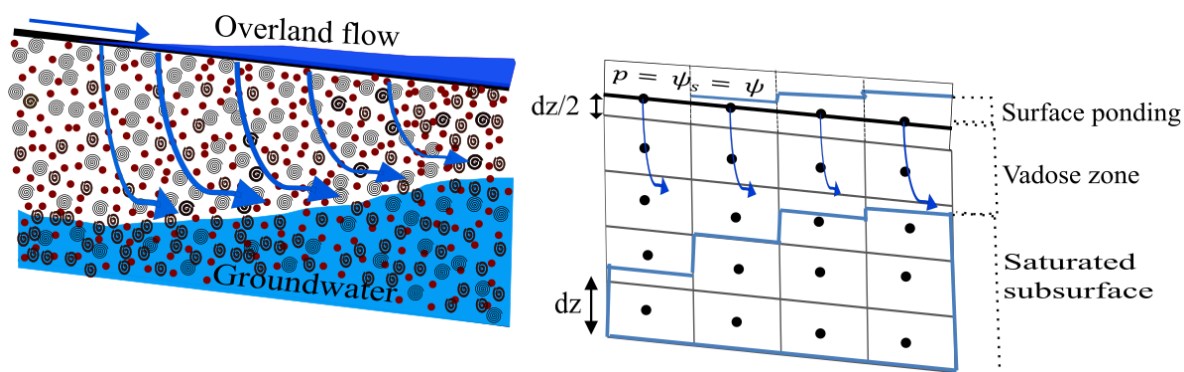
922

923

924   FIGURES

925

926   Figure 1: Coupled surface and subsurface flow systems. The physical system is represented on the

927   left and a schematic of the overland flow boundary condition (continuity of pressure and flux at

928   the ground surface) is on the right. The equation, $p = \psi_s = \psi$ in Figure 1 signifies that at the

929   ground surface, the vertically averaged surface pressure and subsurface pressure head are equal,

930   which is the unique overland flow boundary used by ParFlow.

931

932
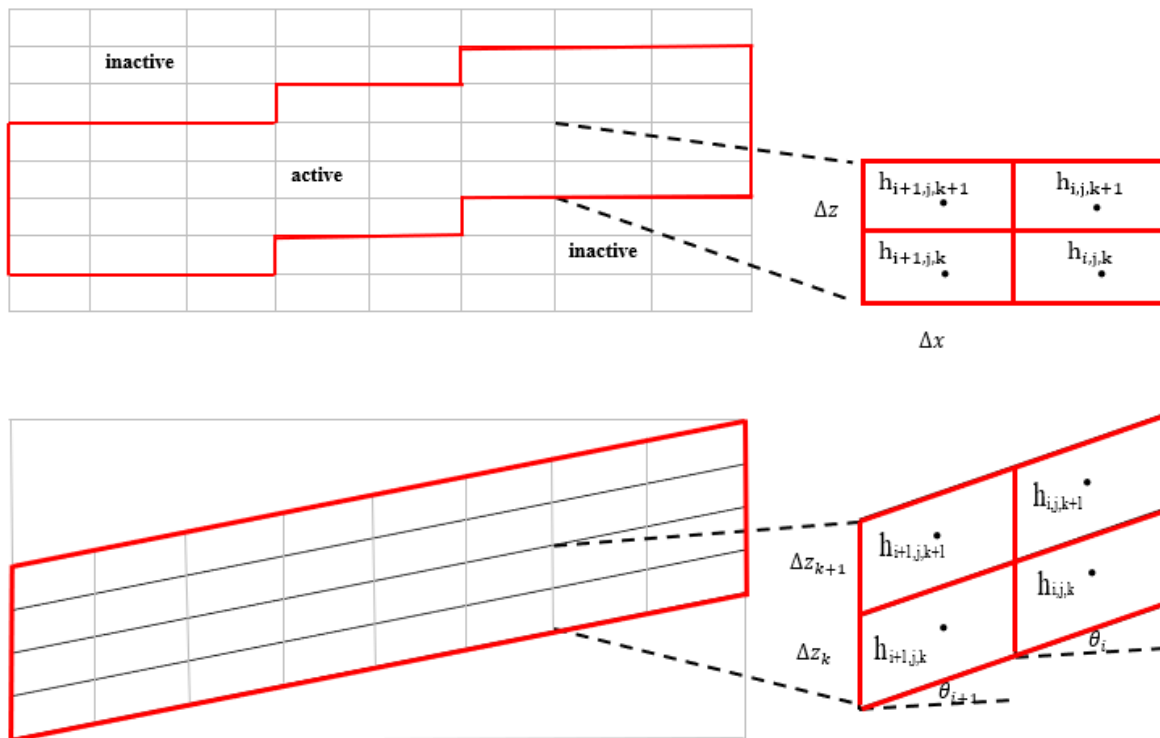
933

934 Figure 2: Representation of orthogonal (upper) and the terrain following (lower) grid formulations

935 and schematics of the associated finite difference dependences (right). The i, j, and k are the x, y,

936 and z cell indices

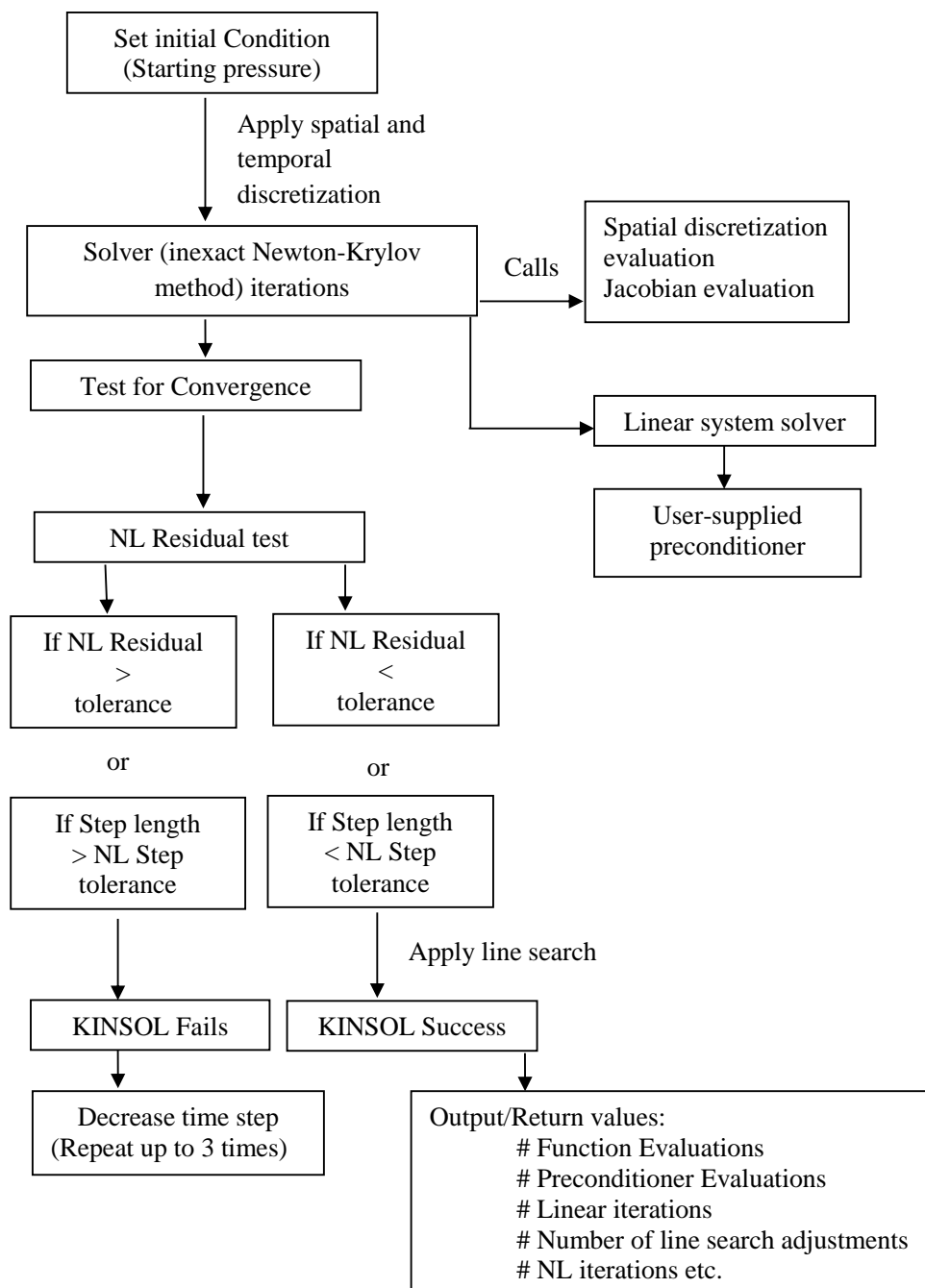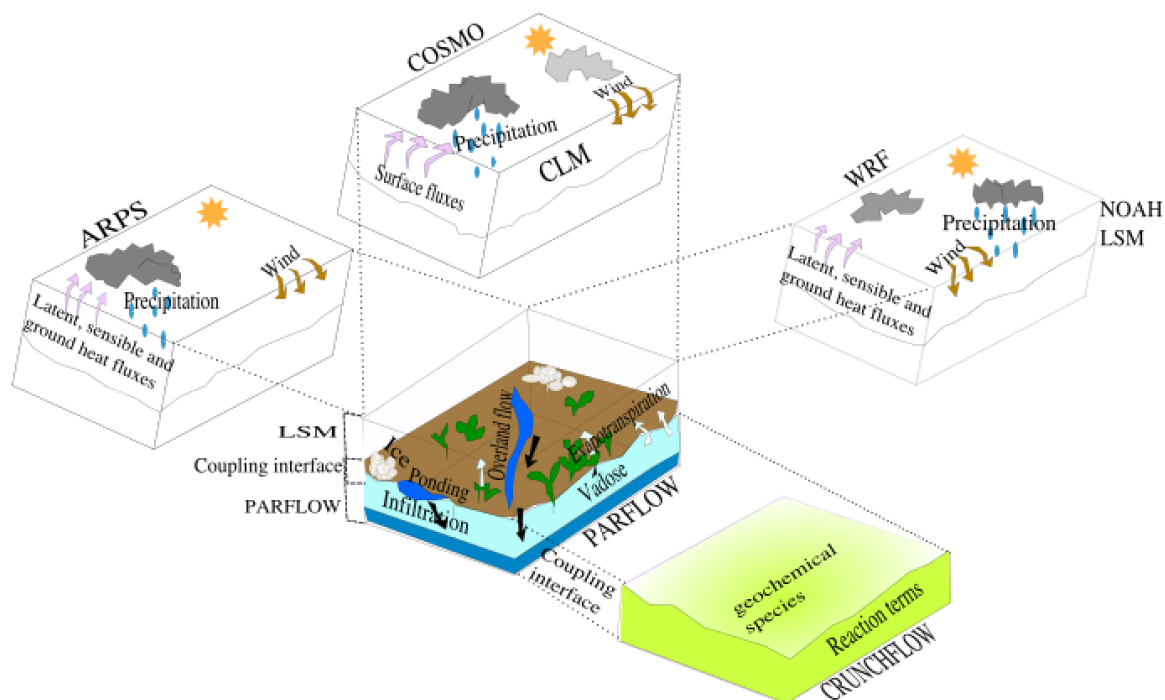937

938

939

940

941

942

943

944

945

946

947

948

949

950

951

952

953

954

955

956

957

958

959

960

961

962

963

964

965 Figure 3: Working flow chart of ParFlow's solver for linear and non-linear system solution

966

967
968   Figure 4(a): A pictorial description of the relevant physical environmental features and model

969   coupling. CLM represents the Community Land Model, a stand-alone Land Surface Model (LSM)

970   via which ParFlow couples' COSMO. The modified version of CLM by Dai et al., (2003) and is

971   not shown in Figure 4(a) because it is a module only for ParFlow, not really a stand-alone LSM

972   any longer. The core model (ParFlow) always solves the variably saturated 3-D groundwater flow

973   problem but the various couplings add additional capabilities.

974
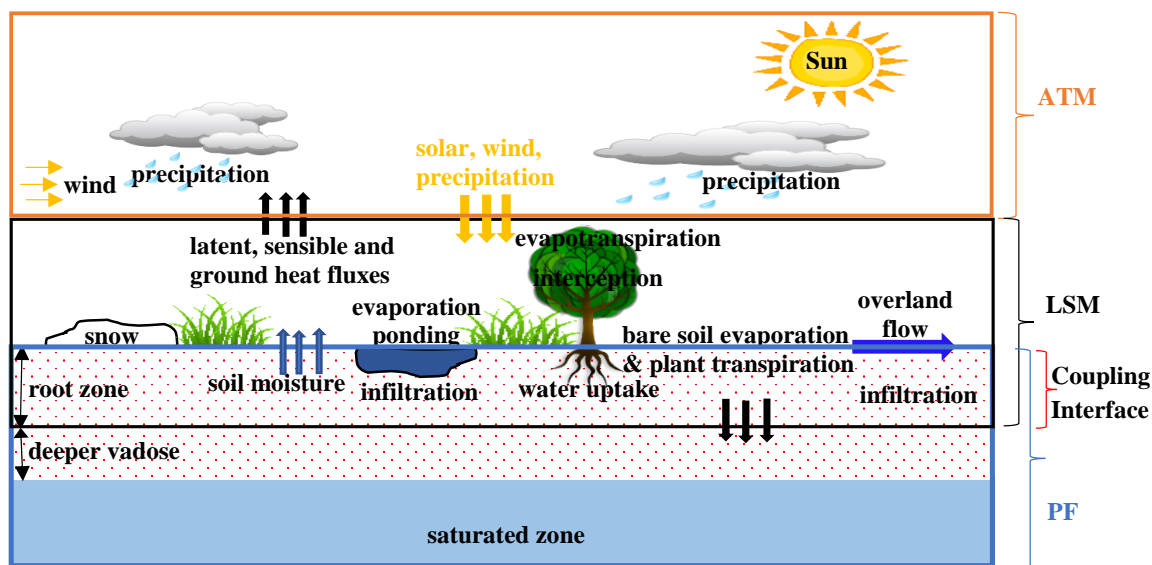
975

976

977

978
979
980
981
982
983
984
985
986
987
988
989

990 Figure 4(b): Schematic showing information transmission at the coupling interface. PF, LSM, and

991 ATM indicate the portions of the physical system simulated by ParFlow, Land Surface Models,

992 and Atmospheric Models respectively. The downward and upward arrows indicate the directions

993 of information transmission between adjacent models. Note: Coupling between ParFlow and

994 CrunchFlow (not shown) occur within the subsurface.

995

996

997

998

999

1000
1001
1002
1003
1004
1005
1006
1007
1008
1009

ParFlow
Atmospheric Models with LSM
LSMs
CrunchFlow
Model Coupler
Atmospheric Models

COSMO
OASIS3
CLM
WRF
ARPS
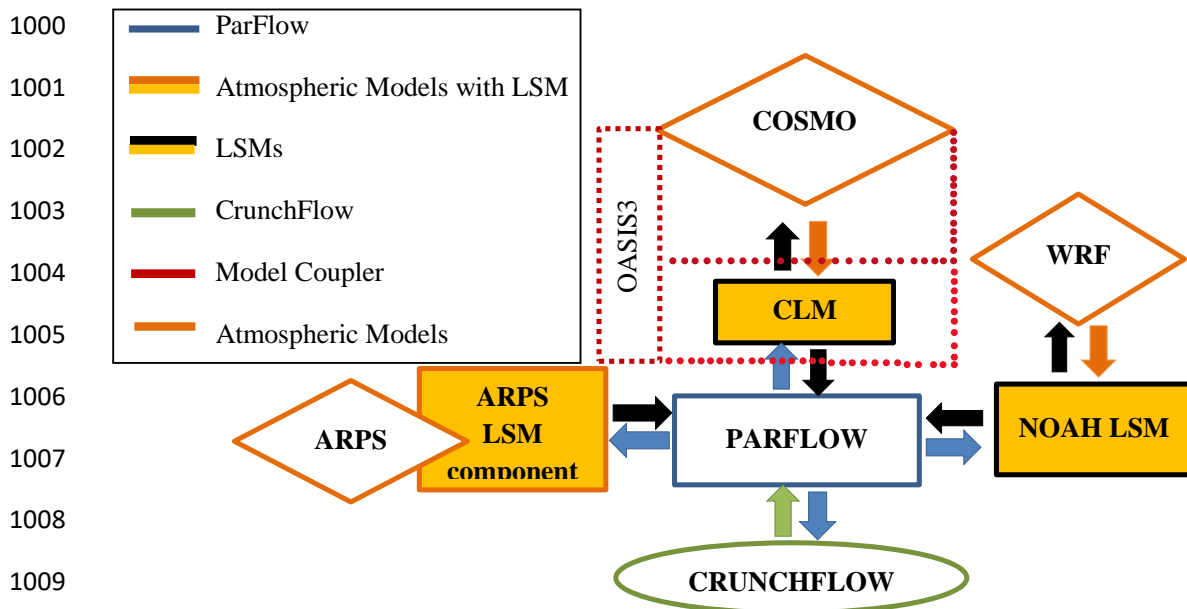ARPS LSM component
PARFLOW
NOAH LSM
CRUNCHFLOW

Figure 5: Schematic of the communication structure of the coupled models. Note: CLM represents a stand-alone Community Land Model. The modified version of Common Land Model by Dai et al., (2003) is not shown here because it is a module only for ParFlow, not really a stand-alone LSM any longer.

1010
1011
1012
1013
1014
1015
1016
1017
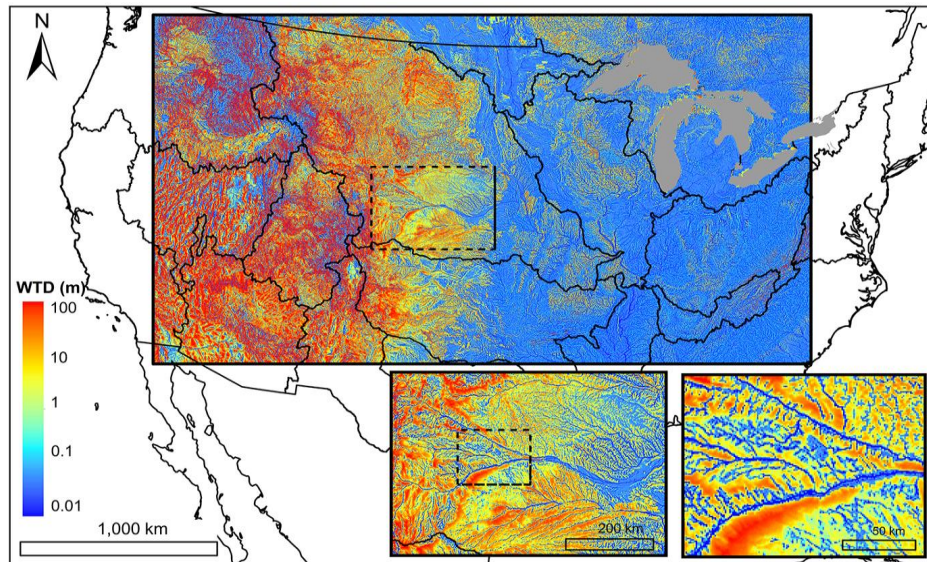
1018

1019   Figure 6: Map of water table depth (m) over the simulation domain with two insets zooming into

1020   the North and South Platte River basin, headwaters to the Mississippi River. Colors represent depth

1021   in log scale (from 0.01 to 100 m) (reproduced from Maxwell et al., 2015). The domain uses 1km^2

1022   grid cells and represents one of the largest, and highest resolution domains simulated by integrated

1023   models to date.

1024
1025

1026

East Inlet watershed, CO
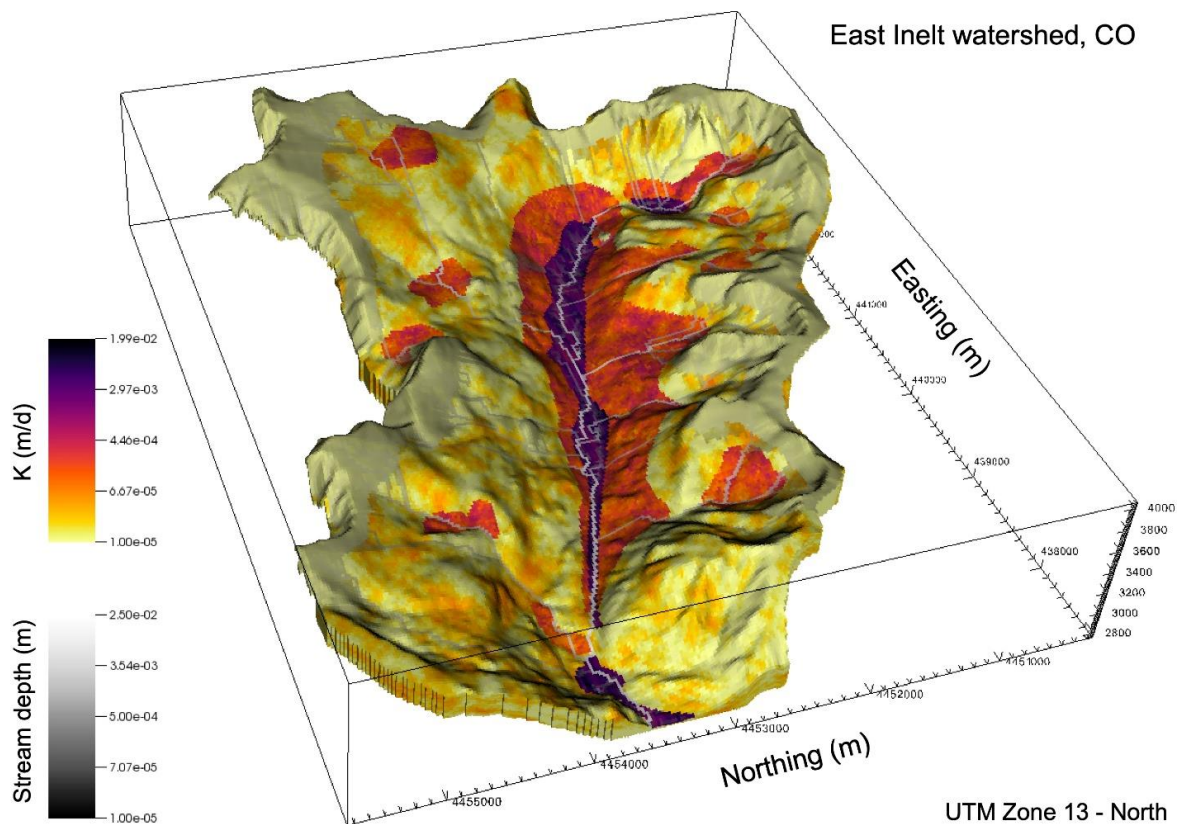
1027

1028

1029 Figure 7: Map of hydraulic conductivity (K) and stream depth in the East Inlet watershed in

1030 Colorado (Engdahl and Maxwell, 2015). This domain covers 30km^2 using 3.1 million 20m^2 (lateral

1031 grid cells. The springs emanating from within the hillslopes highlight the realism afforded by

1032 integrated modeling at small scales.

1033

1034

1035

Geoscientific
Model Development
Discussions

1036   Table 1: Details for the various scaling studies conducted using ParFlow

Simulation Case	Computer System	Processor Number	Jacobian/ Numerical Method	Preconditioner	Computation time (seconds)	Problem Size (cell Number)	Parallel Efficiency (%)	Study
Surface processes and variably saturated flow (ParFlow and CLM)	JUGENE (IBM Blue-Gene Super-computer)	16,384	Finite difference	ParFlow Multigrid	10,920	486,000	58.00	(Kollet et al., 2010)
Terrain Following Grid	JUGENE (IBM Blue-Gene Super-computer)	4,096	Analytical	Non-Symmetric	1,130.50	2,048,000,000	80.91	(Maxwell, 2013)
Overland flow	Intel Xeon Tightly coupled Linux Cluster	100	Finite difference	–	10,800	50,000	82.00	(Kollet and Maxwell, 2006)
Excess infiltration produced runoff	Intel Xeon Tightly coupled Linux Cluster	100	Finite difference	–	10,800	50,000	72.00	(Kollet and Maxwell, 2006)
Terrain Following Grid	JUGENE (IBM Blue-Gene Super-computer)	16,384	Finite difference	Symmetric	2,100.81	8,192,000,000	50.60	(Maxwell, 2013)
Subsurface and Overland flow coupling	IBM BGQ architecture	1,024	Analytical /Finite difference	ParFlow Multigrid	7,200	150,000	50.00	(Osei-Kuffuor et al., 2014)
Fully coupling terrestrial systems modeling platform	IBM BGQ system JUQUEEN	4,096	–	–	–	38,880	82.00	(Gasper et al., 2014)
Performance evaluation of ParFlow code (modified version of ParFlow)	(IBM Blue-Gene Super-computer) JUQUEEN	458,752	Finite difference	–	–	10,569,646,080	–	(Burstedde et al., 2018)

Note: The hyphen "–" "shows that information was not provided by the appropriate study

1037

1038

1039 Table 2: Selected coupling studies involving application of ParFlow and atmospheric, land surface, and subsurface models

Application	Coupled Model	Simulation Scale	Study
Surface heterogeneity, surface energy budget	CLM	Urban watershed Ballona Creek watershed, CA	(Reyes et al., 2016)
Sensitivity analysis (evaporation parameterization)	CLM (modified)	Column	(Jefferson and Maxwell, 2015)
Sensitivity of photosynthesis and stomatal resistivity parameters	CLM (modified)	Column	(Jefferson et al., 2017)
Active subspaces; dimension reduction; energy fluxes	CLM (modified)	Hillslope	(Jefferson et al., 2015)
Spin-up behavior; initial conditions watershed	CLM	Regional	(Seck et al., 2015)
Urban processes	CLM	Regional	(Bhaskar et al., 2015)
Global sensitivity	CLM	watershed	(Srivastava et al., 2014)
Entropy production optimization and inference principles	CLM	Hillslope	(Kollet, 2015)
Soil moisture dynamics	CLM	Catchment	(Fang etal., 2015)
Dual-boundary forcing concept	CLM	Catchment	(Rahman et al., 2015)
Initial conditions; Spin–up	CLM	Catchment; Watershed	(Ajami et al., 2014, 2015)
Groundwater-fed irrigation impacts of natural systems; optimization water allocation algorithm	CLM	Watershed; Sub-watershed	(Condon and Maxwell, 2013, 2014)
Subsurface heterogeneity (land surface fluxes)	CLM	Watershed	(Condon et al., 2013)
Mountain Pine Beetle	CLM	Hillslope	(Mikkelson et al., 2013)
Groundwater-land surface-atmosphere feedbacks	CLM	Watershed	(Ferguson and Maxwell, 2010, 2011, 2012)
Subsurface heterogeneity (land surface processes)	CLM	Hillslope	(Atchley and Maxwell, 2011)
Computational scaling	CLM	Hillslope	(Kollet et al., 2010)
Subsurface heterogeneity (infiltration in arid environment)	CLM	Hillslope	(Maxwell, 2010)
Subsurface heterogeneity (land energy fluxes)	CLM	Hillslope	(Rihani et al., 2010)
Heat and subsurface energy transport (ParFlowE)	CLM	Column	(Kollet et al., 2009)
Subsurface heterogeneity on evapotranspiration	CLM	Column, Hillslope	(Kollet, 2009)
Subsurface heterogeneity (land-energy fluxes; runoff)	CLM	Watershed; Hillslope	(Kollet and Maxwell, 2008)
Climate change (land-energy feedbacks to groundwater)	CLM	Watershed	(Maxwell and Kollet, 2008)
Model development	CLM	Column	(Maxwell and Miller, 2005)
Subsurface transport	CLM	Aquifer	(Tompson et al., 1998, 1999; Maxwell et al., 2003)
Model development (TerrSysMP)	COSMO	Watershed	(Shrestha et al., 2014)
Implementation and Scaling (TerrSysMP)	COSMO	Continental	(Gasper et al., 2014)

Geoscientific
Model Development
Discussions
Open Access

Groundwater response to ground surface-atmosphere feedbacks	COSMO	European CORDEX domain (Continental)	(Keune et al., 2016)
Atmosphere, DART, data assimilation	WRF	Watershed	(Williams et al., 2013)
Coupled model development (Atmosphere)	WRF	Watershed	(Maxwell et al., 2011)
Subsurface heterogeneity (runoff generation)	WRF	Hillslope	(Meyerhoff and Maxwell, 2010)
Subsurface uncertainty to the atmosphere	WRF	Watershed	(Williams and Maxwell, 2011)
Subsurface transport	ARPS	Watershed	(Maxwell et al., 2007)
Terrain and soil moisture heterogeneity on atmosphere	ARPS	Hillslope	(Rihani et al., 2015)
Risk Assessment of CO leakage	CRUNCHFLOW	Aquifer	(Atchley et al., 2013)
Reactive transport heterogeneous saturated subsurface environment	CRUNCHFLOW	Aquifer	(Beisman et al., 2015)

Note: "CLM" show that coupling with ParFlow was by the original Common Land Model or Community Land Model. "CLM (modified)" show that the modified version of Common Land Model by (Dai et al., 2003) was a module for ParFlow.

1040
1041

References

Abu-El-Sha'r, W. Y., and Rihani, J. F.: Application of the high performance computing techniques of parflow simulator to model groundwater flow at Azraq basin, Water Resour. Manag., 21(2), 409–425, doi:10.1007/s11269-006-9023-5, 2007.

Ajami, H., M. F. McCabe, Evans, J. P., and Stisen, S.: Assessing the impact of model spin-up on surface water-groundwater interactions using an integrated hydrologic model, Water Resour. Res., 50, 1–21, doi:10.1002/2013WR014258.Received, 2014.

Ajami, H., McCabe, M. F., and Evans, J. P.: Impacts of model initialization on an integrated surface water-groundwater model, Hydrol. Process., 29(17), 3790–3801, doi:10.1002/hyp.10478, 2015.

Allievi, A., and Calisal, S. M.: Application of Bubnov-Galerkin formulation to orthogonal grid generation, J. Comput. Phys., 98(1), 163–173, doi:10.1016/0021-9991(92)90181-W, 1992.

Amdahl, G. M.: Validity of the single processor approach to achieving large scale computing capabilities, in spring joint computer conference, vol. 37, 256–9, 1967.

Anyah, R. O., Weaver, C. P., Miguez-Macho, G., Fan, Y., and Robock, A.: Incorporating water table dynamics in climate modeling: 3. Simulated groundwater influence on coupled land-atmosphere variability, J. Geophys. Res. Atmos., 113(7), 1–15, doi:10.1029/2007JD009087, 2008.

Ashby, S. F., and Falgout, R. D.: A Parallel Multigrid Preconditioned Conjugate Gradient Algorithm for Groundwater Flow Simulations, Nucl. Sci. Eng., 124, 145–159, 1996.

Ashby, S. F., Falgout, R. D., Smith, S. G., and Tompson, A. F. B.: Modeling groundwater flow on MPPs, Proc. Scalable Parallel Libr. Conf., 17–25, doi:10.1109/SPLC.1993.365586, 1993.

Ashby, S. F., Falgout, R. D., Tompson, A., and Fogwell, T.: Numerical simulation of groundwater flow on MPPs, , 17–25, 1994.

Ashby, S. F., Falgout, R. D., and Tompson, A. F. B.: A Scalable Approach to Modeling Groundwater Flow on Massively Parallel Computers, in In Next Generation Environmental Models and Computational Methods, vol. 87, 201, 1997.

Atchley, A. L., and Maxwell, R. M.: Influences of subsurface heterogeneity and vegetation cover on soil moisture, surface temperature and evapotranspiration at hillslope scales, Hydrogeol. J., 19(2), 289–305, doi:10.1007/s10040-010-0690-1, 2011.

Atchley, A. L., Maxwell, R. M., and Navarre-Sitchler, A. K.,:Human health risk assessment of CO_2 leakage into overlying aquifers using a stochastic, geochemical reactive transport approach, Environ. Sci. Technol., 47(11), 5954–5962, doi:10.1021/es400316c, 2013.

Baldauf, M., Seifert, A., Forstner, J., Majewski, D., and Raschendorfer, M.: Operational Convective-Scale Numerical Weather Prediction with the COSMO Model : Description and Sensitivities, Am. Meteorol. Soc., 3887–3905, doi:10.1175/MWR-D-10-05013.1, 2011.

Beisman, J.: Development of a parallel reactive transport model with spatially variable nitrate reduction in a floodplain aquifer, 2007.

Beisman, J. J., Maxwell, R. M., Steefel, C. I., and Molins, S.: ParCrunchFlow : an efficient , parallel reactive transport simulation tool for physically and chemically heterogeneous saturated subsurface environments, 403–422, doi:10.1007/s10596-015-9475-x, 2015a.

Beisman, J. J., Maxwell, R. M., Navarre-Sitchler, A. K., Steefel, C. I., and Molins, S.: ParCrunchFlow: an efficient, parallel reactive transport simulation tool for physically and chemically heterogeneous saturated subsurface environments, Comput. Geosci., 19(2), 403–

1087   422, doi:10.1007/s10596-015-9475-x, 2015b.

1088 Bell, J. B., Dawson, C. N., and Shubin, G. R.: An unsplit, higher order godunov method for
1089   scalar conservation laws in multiple dimensions, J. Comput. Phys., 74(1), 1–24,
1090   doi:10.1016/0021-9991(88)90065-4, 1988.

1091 Benson, D. A., Aquino, T., Bolster, D. N. E. C, and Christopher, D. F.G., Henri, V.: A
1092   comparison of Eulerian and Lagrangian transport and non-linear reaction algorithms, Adv.
1093   Water Resour., 99, 15–37, 2017.

1094 Bettems, J. M., Asensio, H., Bonafe, Duniec, G., Fuhrer, O., Helmert, J., Heret, C., Kazakova,
1095   E., Lange, Machulskaya, E., Mazur, A., De Morsier, G., Rianna, G., Rozinkina, I., Vieli, B.,
1096   Vogel, G.:The COSMO Priority Project "COLOBOC": Final Technical Report No 27, (No
1097   27), 2015.

1098 Beven, K.: Robert E. Horton's perceptual model of infiltration processes, Hydrol. Process.,
1099   18(17), 3447–3460, doi:10.1002/hyp.5740, 2004.

1100 Bhaskar, A. S., Welty, C., Maxwell, R. M., and Miller, A. J.: Untangling the effects of urban
1101   development on subsurface storage in Baltimore, Water Resour. Res., 51(2), 1158–1181,
1102   doi:10.1002/2014WR016039, 2015.

1103 Bixio, A. C., Gambolati, A. G., Paniconi, A. C., Putti, A. M., Shestopalov, A. V. M., Bublias, V.
1104   N., Bohuslavsky, A. A. S., Kasteltseva, A. N. B., and Rudenko, Y. F.: Modeling
1105   groundwater-surface water interactions including effects of morphogenetic depressions in
1106   the Chernobyl exclusion zone, Environ. Geol., 42(162–177), doi:10.1007/s00254-001-0486-
1107   7, 2002.

1108 Briggs, W. L., Henson, V. E., and McCormick, S. F.: A Multigrid Tutorial, Second Edition,
1109   2000.

1110 Brookfield, A. E., Sudicky, E. A., Park, Y. J., and Conant, B.: Thermal transport modelling in a
1111   fully integrated surface/subsurface framework, Hydrol. Process., 23(15), 2150–2164,
1112   doi:10.1002/hyp.7282, 2009.

1113 Brown, P. N., and Saad, Y.: Hybrid Krylov Methods for Nonlinear Systems of Equations, SIAM
1114   J. Sci. Stat. Comput., 11(3), 450–481, doi:10.1137/0911026, 1990.

1115 Burstedde, C., Fonseca, J. A., and Kollet, S.: Enhancing speed and scalability of the ParFlow
1116   simulation code, Comput. Geosci., 22(1), 347–361, doi:10.1007/s10596-017-9696-2, 2018.

1117 Camporese, M., Paniconi, C., Putti, M., and Orlandini, S.: Surface-subsurface flow modeling
1118   with path-based runoff routing, boundary condition-based coupling, and assimilation of
1119   multisource observation data, Water Resour. Res., 46(2), doi:10.1029/2008WR007536,
1120   2010.

1121 Castronova, A. M., Goodall, J. L., and Ercan, M. B.: Integrated Modeling within a Hydrologic
1122   Information System: An OpenMI Based Approach, Environ. Model. Softw.,
1123   doi:10.1016/j.envsoft, 2013.

1124 Celia, M. A., Bouloutas, E. T., and Zarba, R. L.: A general mass-conservative numerical
1125   solution for the unsaturated flow equation, Water Resour. Res., 26(7), 1483–1496,
1126   doi:10.1029/WR026i007p01483, 1990.

1127 Chow, F. K., Kollet, S. J., Maxwell, R. M., and Duan, Q.: Effects of Soil Moisture Heterogeneity
1128   on Boundary Layer Flow with Coupled Groundwater, Land-Surface, and Mesoscale
1129   Atmospheric Modeling, 17th Symp. Bound. Laters Turbul., doi:10.1016/j.phrs.2010.10.003,
1130   2006.

1131 Collier, A. M., Hindmarsh, A. C., Serban, R., and Woodward, C. S.: User Documentation for
1132   kinsol v2.8.2 (SUNDIALS v2.6.2), , 1, 120, 2015.

1133 Condon, L. E., and Maxwell, R. M.: Implementation of a linear optimization water allocation
1134   algorithm into a fully integrated physical hydrology model, Adv. Water Resour., 60, 135–
1135   147, doi:10.1016/j.advwatres.2013.07.012, 2013.
1136 Condon, L. E., and Maxwell, R. M.: Groundwater-fed irrigation impacts spatially distributed
1137   temporal scaling behavior of the natural system: a spatio-temporal framework for
1138   understanding water management impacts, Environ. Res. Lett., 9(3), 034009,
1139   doi:10.1088/1748-9326/9/3/034009, 2014.
1140 Condon, L. E., and Maxwell, R.M.: Evaluating the relationship between topography and
1141   groundwater using outputs from a continental-scale integrated hydrology model, Water
1142   Resour. Res., 51(8), 6602–6621, doi:10.1002/2014WR016774, 2015.
1143 Condon, L. E., Maxwell, R. M., and Gangopadhyay, S.: The impact of subsurface
1144   conceptualization on land energy fluxes, Adv. Water Resour., 60, 188–203,
1145   doi:10.1016/J.ADVWATRES.2013.08.001, 2013.
1146 Condon, L. E., Hering, A. S., and Maxwell, R. M.: Quantitative assessment of groundwater
1147   controls across major US river basins using a multi-model regression algorithm, Adv. Water
1148   Resour., 82, 106–123, doi:10.1016/J.ADVWATRES.2015.04.008, 2015.
1149 Dai, Y. et al.: The Common Land Model, Bull. Am. Meteorol. Soc., 84(8), 1013–1023,
1150   doi:10.1175/BAMS-84-8-1013, 2003.
1151 Dembo, R. S., and Eisenstat, S. C.: Inexact newton methods, in SIAM J. Numer. Anal., vol. 19,
1152   pp. 400–408, 1982.
1153 Dennis Jr, John E., and R. B. S.: Numerical Methods for Unconstrained Optimization and
1154   Nonlinear Equations, 1996.
1155 Duniec, G., and Mazur, A.: COLOBOC - MOSAIC parameterization in COSMO model v. 4.8,
1156   (11), 69–81, 2011.
1157 Durbin, P.: An Approach to Local Refinement of Structured Grids An Approach to Local
1158   Refinement of Structured Grids, J. Comput. Phys., 181, 639–653,
1159   doi:10.1006/jcph.2002.7147, 2002.
1160 Eca, L.: 2D orthogonal grid generation with boundary point distribution control, J. Comput.
1161   Phys., 125(2), 440–453, doi:10.1006/jcph.1996.0106, 1996.
1162 Eisenstat, S. C., and Walker, H. F.: Choosing the Forcing Terms in an Inexact Newton Method,
1163   SIAM J. Sci. Comput., 17(1), 16–32, doi:10.1137/0917003, 1996.
1164 Ek, M. B., Mitchell, K. E., Lin, Y., Rogers, E., Grunmann, P., Koren, V., Gayno, G., and
1165   Tarpley, J. D.: Implementation of Noah land surface model advances in the National
1166   Centers for Environmental Prediction operational mesoscale Eta model, J. Geophys. Res.
1167   Atmos., 108(D22), doi:10.1029/2002JD003296, 2003.
1168 Engdahl, N. B., and Maxwell, R. M.: Quantifying changes in age distributions and the
1169   hydrologic balance of a high-mountain watershed from climate induced variations in
1170   recharge, J. Hydrol., 522, 152–162, doi:10.1016/j.jhydrol.2014.12.032, 2015.
1171 Engdahl, N. B., McCallum, J. L., and Massoudieh, A.: Transient age distributions in subsurface
1172   hydrologic systems, J. Hydrol., 543, 88–100, doi:10.1016/J. Hydrol.2016.04.066, 2016.
1173 Falgout, R. D., and Yang, U. M.: Hypre: A Library of High Performance Preconditioners, in
1174   International Conference on Computational Science., 632–641, Springer, Berlin, 2002.
1175 Falgout, R. D., Baldwin, C., Bosl, W., Hornung, R., Shumaker, D., Smith, S., Woodward, C. S.,
1176   and Tompson, A. F. B.: Enabling Computational Technologies for Subsurface Simulations,
1177   1999.
1178 Ferguson, I. M., and Maxwell, R. M.: Groundwater-Land Surface-Atmosphere Feedbacks:

1179   Impacts of Groundwater Pumping and Irrigation on Land-Atmosphere Interactions, Proc.
1180   xviii Int. Conf. Comput. Methods Water Resour., 722–729, 2010.
1181   Ferguson, I. M., and Maxwell, R. M.: Human impacts on terrestrial hydrology: climate change
1182   versus pumping and irrigation, Environ. Res. Lett., 7(4), 044022, doi:10.1088/1748-
1183   9326/7/4/044022, 2012.
1184   Frei, S., Fleckenstein, J. H., Kollet, S. J., and Maxwell, R. M.: Patterns and dynamics of river-
1185   aquifer exchange with variably-saturated flow using a fully-coupled model, J. Hydrol.,
1186   375(3–4), 383–393, doi:10.1016/j.jhydrol.2009.06.038, 2009.
1187   Gasper, F., Goergen, K., Shrestha, P., Sulis, M., Rihani, J., Geimer, M., and Kollet, S. J.:
1188   Implementation and scaling of the fully coupled Terrestrial Systems Modeling Platform
1189   (TerrSysMP v1.0) in a massively parallel supercomputing environment - A case study on
1190   JUQUEEN (IBM Blue Gene/Q), Geosci. Model Dev., 7(5), 2531–2543, doi:10.5194/gmd-
1191   7-2531-2014, 2014.
1192   Gebler, S., Kollet, S., Qu, W., and Vereecken, H.: High resolution modelling of soil moisture
1193   patterns with ParFlow-CLM : Comparison with sensor network data, , 17, 2015, 2015.
1194   Gilbert, J. M., and Maxwell, R. M.: Examining regional groundwater-surface water dynamics
1195   using an integrated hydrologic model of the San Joaquin River basin, Hydrol. Earth Syst.
1196   Sci. Discuss., 1–39, doi:10.5194/hess-2016-488, 2016.
1197   Gustafson, J. L.: Reevaluating amdahl's law, 31(5), 532–533, 1988.
1198   Haussling, H. ., and Coleman, R.: A method for generation of orthogonal and nearly orthogonal
1199   boundary-fitted coordinate systems, J. Comput. Phys., 43(2), 373–381, doi:10.1016/0021-
1200   9991(81)90129-7, 1981.
1201   Hindmarsh, A. C., Brown, P. N., Grant, K. E., Lee, S. L., Serban, R., Shumaker, D. E., and
1202   Woodward, C. S.: SUNDIALS: Suite of nonlinear and differential/algebraic equation
1203   solvers, ACM Trans. Math. Softw., 31(3), 363–396, doi:10.1145/1089014.1089020, 2005.
1204   Ian F. M., Jefferson, J. L., Maxwell, R. M., Kollet, S. J.: Effects of root water uptake formulation
1205   on simulated water and energy budgets at local and basin scales, Env. Earth Sci, 75(316),
1206   doi:DOI 10.1007/s12665-015-5041-z, 2016.
1207   Ivanov, V. Y., Vivoni, E. R., Bras, R. L., and Entekhabi, D.: Catchment hydrologic response
1208   with a fully distributed triangulated irregular network model, Water Resour. Res., 40(11),
1209   1–23, doi:10.1029/2004WR003218, 2014.
1210   Jefferson, J. L., and Maxwell, R. M.: Evaluation of simple to complex parameterizations of bare
1211   ground evaporation, J. Adv. Model. Earth Syst., 7, 1075–1092, doi:10.1002/
1212   2014MS000398. Received, 2015.
1213   Jefferson, J. L., Gilbert, J. M., Constantine, P. G., and Maxwell, R.M.: Active subspaces for
1214   sensitivity analysis and dimension reduction of an integrated hydrologic model, Comput.
1215   Geosci., 83, 127–138, doi:10.1016/j.cageo.2015.07.001, 2015.
1216   Jefferson, J. L., Maxwell,R. M., and Constantine, P. G.: Exploring the Sensitivity of
1217   Photosynthesis and Stomatal Resistance Parameters in a Land Surface Model, J.
1218   Hydrometeorol., 18(3), 897–915, doi:10.1175/JHM-D-16-0053.1, 2017.
1219   Jiang, X., Niu, G. Y., and Yang, Z. L.: Impacts of vegetation and groundwater dynamics on
1220   warm season precipitation over the Central United States, J. Geophys. Res. Atmos., 114(6),
1221   1–15, doi:10.1029/2008JD010756, 2009.
1222   Jones, J. E., and Woodward, C. S.: Preconditioning Newton- Krylov Methods for Variably
1223   Saturated Flow, in 13th International Conference on Computational Methods in Water
1224   Resources, Calgary, Alberta, Canada, 2000.

1225 Jones, J. E., and Woodward, C. S.: Newton-Krylov-multigrid solvers for large-scale, highly
1226   heterogeneous, variably saturated flow problems, Adv. Water Resour., 24(7), 763–774,
1227   doi:10.1016/S0309-1708(00)00075-0, 2001.
1228 Keune, J., Gasper, F., Goergen, K., Hense, A., Shrestha, P., Sulis, M., and Kollet, S.: Studying
1229   the influence of groundwater representations on land surface-atmosphere feedbacks during
1230   the European heat wave in 2003, J. Geophys. Res., 121(22), 13,301-13,325,
1231   doi:10.1002/2016JD025426, 2016.
1232 Khorsandi, E., Kollet, S., Venema, V., and Simmer, C.: Investigating the effect of bottom
1233   boundary condition placement on ground heat storage in climate time scale simulations
1234   using ParflowE, Geophys. Res., 16(4), 2014, doi:10.1029/2006GL028546, 2014.
1235 Kirkner, D. J., and Reeves, H.: Multicomponent Mass Transport With Homogeneous and
1236   Heterogeneous Chemical Reactions' Effect of the Chemistry on the Choice of Numerical
1237   Algorithm 1. Theory, Water Resour. Res., 24(10), 1719–1729, 1988.
1238 Kollet, S., Sulis, M., Maxwell, R. M., Paniconi, C., Putti, M., Bertoldi, G., Coon, E. T., Cordano,
1239   E., Endrizzi, S., Kikinzon, E., Mouche, E., Mugler, C., Young-Jin Park, J. C. Refsgaard,
1240   Stisen Simo, and E. S.: The integrated hydrologic model intercomparison project,IH-MIP2:
1241   A second set of benchmark results to diagnoseintegrated hydrology and feedbacks, Water
1242   Resour. Res., 52(1), 1–20, doi:10.1002/2014WR015716, 2017.
1243 Kollet, S. J.: Influence of soil heterogeneity on evapotranspiration under shallow water table
1244   conditions: transient, stochastic simulations, Environ. Res. Lett., 4, 035007,
1245   doi:10.1088/1748-9326/4/3/035007, 2009.
1246 Kollet, S. J.: Optimality and inference in hydrology from entropy production considerations:
1247   synthetic hillslope numerical experiments., Hydrol. Earth Syst. Sci., 12, 5123–5149, 2015.
1248 Kollet, S. J., and Maxwell, R. M.: Integrated surface-groundwater flow modeling: A free-surface
1249   overland flow boundary condition in a parallel groundwater flow model, Adv. Water
1250   Resour., 29(7), 945–958, doi:10.1016/j.advwatres.2005.08.006, 2006.
1251 Kollet, S. J., and Maxwell, R. M.: Capturing the influence of groundwater dynamics on land
1252   surface processes using an integrated, distributed watershed model, Water Resour. Res.,
1253   44(2), 1–18, doi:10.1029/2007WR006004, 2008a.
1254 Kollet, S. J., and Maxwell, R. M.: Demonstrating fractal scaling of baseflow residence time
1255   distributions using a fully-coupled groundwater and land surface model, Geophys. Res.
1256   Lett., 35(7), 1–6, doi:10.1029/2008GL033215, 2008b.
1257 Kollet, S. J., Cvijanovic, I., Schüttemeyer, D., Maxwell, R. M., Moene, A. F., and Bayer, P.: The
1258   Influence of Rain Sensible Heat and Subsurface Energy Transport on the Energy Balance at
1259   the Land Surface, Vadose Zo. J., 8(4), 846, doi:10.2136/vzj2009.0005, 2009.
1260 Kollet, S. J., Maxwell, R. M., Woodward, C. S., Smith, S., Vanderborght, J., Vereecken, H., and
1261   Simmer, C.: Proof of concept of regional scale hydrologic simulations at hydrologic
1262   resolution utilizing massively parallel computer resources, Water Resour. Res., 46(4), 1–7,
1263   doi:10.1029/2009WR008730, 2010.
1264 Kumar, M., Duffy, C. J., and Salvage, K. M.: A second-order accurate, finite volume–based,
1265   integrated hydrologic modeling (FIHM) framework for simulation of surface and subsurface
1266   flow, Vadose Zo. J., 8(4), 873, doi:10.2136/vzj2009.0014, 2009.
1267 LaBolle, E. M., Ahmed, A. A., and Fogg, G. E.: Review of the Integrated Groundwater and
1268   Surface-Water Model (IGSM), Ground Water, 41(2), 238–246, doi:10.1111/j.1745-
1269   6584.2003.tb02587.x, 2003.
1270 Levis, S., and Jaeger, E. B.: COSMO-CLM2 : a new version of the COSMO- CLM model

Geoscientific
Model Development
Discussions

EGU

1271   coupled to the Community Land Model coupled to the Community Land Model, Clim.
1272   Dyn., 37(November), 1889–1907, doi:10.1007/s00382-011-1019-z, 2011.
1273   Li, et al.: Effects of physical and geochemical heterogeneities on mineral transformation and
1274   biomass accumulation during uranium bioremediation at Rifle, Colorado, J. Contam.
1275   Hydrol., 11, 45–63, 2010.
1276   Li, L., Steefel, C. I., and Yang, L.: Scale dependence of mineral dissolution rates within single
1277   pores and fractures, Geochim. Cosmochim. Acta, 72, 360–377,
1278   doi:10.1016/j.gca.2007.10.027, 2007.
1279   Markstrom, S. L., Niswonger, R. G., Regan, R. S., Prudic, D. E., and Barlow, P. M.:
1280   GSFLOW—Coupled Ground-Water and Surface-Water Flow Model Based on the
1281   Integration of the Precipitation-Runoff Modeling System (PRMS) and the Modular Ground-
1282   Water Flow Model (MODFLOW-2005), U.S. Geol. Surv., (Techniques and Methods 6-D1),
1283   240, 2008.
1284   Maxwell, R. M., and Miller, N. L.: Development of a Coupled Land Surface and Groundwater
1285   Model, J. Hydrometeorol., 6, 233–247, doi:10.1175/JHM422.1, 2005.
1286   Maxwell, R. M.: Infiltration in Arid Environments: Spatial Patterns between Subsurface
1287   Heterogeneity and Water-Energy Balances, Vadose Zo. J., 9(4), 970,
1288   doi:10.2136/vzj2010.0014, 2010.
1289   Maxwell, R. M.: A terrain-following grid transform and preconditioner for parallel, large-scale,
1290   integrated hydrologic modeling, Adv. Water Resour., 53, 109–117,
1291   doi:10.1016/j.advwatres.2012.10.001, 2013.
1292   Maxwell, R. M., Welty, C., and Tompson, A. F. B.: Streamline-based simulation of virus
1293   transport resulting from long term artificial recharge in a heterogeneous aquifer, Adv. Water
1294   Resour., 26(10), 1075–1096, doi:10.1016/S0309-1708(03)00074-5, 2003.
1295   Maxwell, R. M., Chow, F. K., and Kollet, S. J.: The groundwater–land-surface–atmosphere
1296   connection: Soil moisture effects on the atmospheric boundary layer in fully-coupled
1297   simulations, Adv. Water Resour., 30(12), 2447–2466, doi:10.1016/j.advwatres.2007.05.018,
1298   2007.
1299   Maxwell, R. M., Lundquist, J. K., Mirocha, J. D., Smith, S. G., Woodward, C. S., and Tompson,
1300   A. F. B.: Development of a Coupled Groundwater–Atmosphere Model, Mon. Weather Rev.,
1301   139(1), 96–116, doi:10.1175/2010MWR3392.1, 2011.
1302   Maxwell, R. M., Condon, L. E., and Kollet, S. J.: A high-resolution simulation of groundwater
1303   and surface water over most of the continental US with the integrated hydrologic model
1304   ParFlow v3, Geosci. Model Dev, 923–937, doi:10.5194/gmd-8-923-2015, 2015.
1305   Maxwell, R. M. et al.: ParFlow User 's Manual, 2016.
1306   Meehl, G. A., Covey, C., McAvaney, B., Latif, M., and Stouffer, R. J.: Overview of the coupled
1307   model intercomparison project, Bull. Am. Meteorol. Soc., 86(1), 89–93,
1308   doi:10.1175/BAMS-86-1-89, 2005.
1309   Meyerhoff, S. B., and Maxwell, R. M.: Using an integrated surface-subsurface model to simulate
1310   runoff from heterogeneous hillslopes, in xviii International Conference on Water Resources,
1311   CIMNE, Barcelona, 2010.
1312   Michalakes, J., Dudhia, J., Gill, D., Klemp, J., and Skamarock, W.: Design of a next-generation
1313   regional weather research and forecast model, Towar. Teracomputing, 19999.
1314   Michalakes, J., Chen, S., Dudhia, J., Hart, L., Klemp, J., Middlecoff, J., and Skamarock, W.:
1315   Development of a next-generation regional weather research and forecast model, Towar.
1316   Teracomputing, 2001.

Geoscientific
Model Development
Discussions

1317 Mikkelson, K. M., Maxwell, R. M., Ferguson, I., Stednick, J. D., Mccray, J. E., and Sharp, J. O.:
1318   Mountain pine beetle infestation impacts: Modeling water and energy budgets at the hill-
1319   slope scale, Ecohydrology, 6(1), 64–72, doi:10.1002/eco.278, 2013.
1320 Mironov, D., Heise, E., Kourzeneva, E. and Ritter, B.: Implementation of the lake
1321   parameterisation scheme FLake into the numerical weather prediction model COSMO,
1322   Boreal Environ. Res., 6095(April), 218–230, 2010.
1323 Mobley, C. D., and Stewart, R. S.: On the numerical generation of boundary-fitted orthogonal
1324   curvilinear coordinate systems, J. Comput. Phys., 34(1), 124–135, doi:10.1016/0021-
1325   9991(80)90117-5, 1980.
1326 Molders, N., and Ruhaak, W.: On the impact of explicitly predicted runoff on the simulated
1327   atmospheric response to small-scale land-use changes—an integrated modeling approach,
1328   Atmos. Res., 63, 2002.
1329 Navarre-Sitchler, A., Steefel, C. I., Sak, P. B., and Brantley, S. L.: A reactive-transport model for
1330   weathering rind formation on basalt, Geochim. Cosmochim. Acta, 75, 7644–7667,
1331   doi:10.1016/j.gca.2011.09.033, 2011.
1332 Oleson, K. W. et al.: Improvements to the Community Land Model and their impact on the
1333   hydrological cycle, J. Geophys. Res. Biogeosciences, 113(G1), doi:10.1029/2007JG000563,
1334   2008.
1335 Osei-Kuffuor, D., Maxwell, R. M., and Woodward, C. S.: Improved numerical solvers for
1336   implicit coupling of subsurface and overland flow, Adv. Water Resour., 74,
1337   doi:10.1016/j.advwatres.2014.09.006, 2014.
1338 Panday, S., and Huyakorn, P. S.: A fully coupled physically-based spatially-distributed model for
1339   evaluating surface/subsurface flow, Adv. Water Resour., 27(4), 361–382,
1340   doi:10.1016/j.advwatres.2004.02.016, 2004.
1341 Rahman, M., Sulis, M., and Kollet, S. J.: Evaluating the dual-boundary forcing concept in
1342   subsurface-land surface interactions of the hydrological cycle, Hydrol. Process., 30(10),
1343   1563–1573, doi:10.1002/hyp.10702, 2016.
1344 Ren, D., and Xue, M.: A revised force–restore model for land surface modeling, Am. Meteorol.
1345   Soc, 2004.
1346 Reyes, B., Maxwell, R. M,. and Hogue, T. S.: Impact of lateral flow and spatial scaling on the
1347   simulation of semi-arid urban land surfaces in an integrated hydrologic and land surface
1348   model, Hydrol. Process., 30(8), 1192–1207, doi:10.1002/hyp.10683, 2016.
1349 Richards, L. A.: Capillary conduction of liquids through porous mediums, J. Appl. Phys., 1(5),
1350   318–333, doi:10.1063/1.1745010, 1931.
1351 Rigon, R., Bertoldi, G., and Over, T. M.: GEOtop: A Distributed Hydrological Model with
1352   Coupled Water and Energy Budgets, J. Hydrometeorol., 7(3), 371–388,
1353   doi:10.1175/jhm497.1, 2006.
1354 Rihani, J.,F., Chow, F. K., Fotini K., and Maxwell, R. M.: Isolating effects of terrain and soil
1355   moisture heterogeneity on the atmospheric boundary layer: Idealized simulations to
1356   diagnose land-atmosphere feedbacks, J. Adv. Model. Earth Syst., 6, 513–526,
1357   doi:10.1002/2014MS000371.Received, 2015.
1358 Rihani, J. F., Maxwell, M. R., and Chow, F. K.: Coupling groundwater and land surface
1359   processes: Idealized simulations to identify effects of terrain and subsurface heterogeneity
1360   on land surface energy fluxes, Water Resour. Res., 46(12), 1–14,
1361   doi:10.1029/2010WR009111, 2010.
1362 Ryskin, G., and Leal, L.: Orthogonal mapping, J. Comput. Phys., 50(1), 71–100,

1363   doi:10.1016/0021-9991(83)90042-6, 1983.
1364   Saad, Y., and Schultz, M. H.: GMRES: A Generalized Minimal Residual Algorithm for Solving
1365   Nonsymmetric Linear Systems, SIAM J. Sci. Stat. Comput., 7(3), 856–869,
1366   doi:10.1137/0907058, 1986.
1367   Seck, A., Welty, C., and Maxwell, R. M.: Spin-up behavior and effects of initial conditions for
1368   an integrated hydrologicmodel Alimatou, Water Resour. Res., 51, 2188–2210,
1369   doi:10.1002/2014WR016371.Received, 2015.
1370   Seuffert, G., Gross, P., Simmer, A. C., and Wood, E. F.: The Influence of Hydrologic Modeling
1371   on the Predicted Local Weather: Two-Way Coupling of a Mesoscale Weather Prediction
1372   Model and a Land Surface Hydrologic Model, J. Hydrometeorol., 3, 2002.
1373   Shen, C., and Phanikumar, M. S.: A process-based, distributed hydrologic model based on a
1374   large-scale method for surface-subsurface coupling, Adv. Water Resour., 33(12), 1524–
1375   1541, doi:10.1016/j.advwatres.2010.09.002, 2010.
1376   Shi, Y., Davis, K. J., Zhang, F., and Duffy, C. J.: Evaluation of the Parameter Sensitivities of a
1377   Coupled Land Surface Hydrologic Model at a Critical Zone Observatory, J.
1378   Hydrometeorol., 15(1), 279–299, doi:10.1175/JHM-D-12-0177.1, 2014.
1379   Shrestha, P., Sulis, M., Masbou, M., Kollet, S., and Simmer, C.: A Scale-Consistent Terrestrial
1380   Systems Modeling Platform Based on COSMO, CLM, and ParFlow, Mon. Weather Rev.,
1381   142, doi:10.1175/MWR-D-14-00029.1, 2014.
1382   Shrestha, P., Sulis, M., Simmer, C., and Kollet, S.: Impacts of grid resolution on surface energy
1383   fluxes simulated with an integrated surface-groundwater flow model, Hydrol. Earth Syst.
1384   Sci, 19, 4317–4326, doi:10.5194/hess-19-4317-2015, 2015.
1385   Simmer, C. et al.: Monitoring and modeling the terrestrial system from pores to catchments: The
1386   transregional collaborative research center on patterns in the soil-vegetation-atmosphere
1387   system, Bull. Am. Meteorol. Soc., 96(10), 1765–1787, doi:10.1175/BAMS-D-13-00134.1,
1388   2015.
1389   Skamarock, W. C., and Klemp, J. B.: A Time-Split Nonhydrostatic AtmosphericModel
1390   forWeather Research and Forecasting Applications, , (001), 1–43, 2007.
1391   Skamarock, W. C., Klemp, J. B., Dudhia, J., Gill, D. O., Barker, D. M., Wang, W., and Powers,
1392   J. G.: A description of the advanced research WRF Version 2, 2005.
1393   Smith, S. G., Ashby, S. F., Falgout, R. D., and Tompsom, A. F. B.: The parallel performance of a
1394   groundwater flow code on the CRAY T3D. In Proceedings of the Seventh SIAM
1395   Conference on Parallel Processing for Scientific Computing, 131, 1995.
1396   Srivastava, V., Graham, W., Muñoz-Carpena, R., and Maxwell, R. M.: Insights on geologic and
1397   vegetative controls over hydrologic behavior of a large complex basin – Global Sensitivity
1398   Analysis of an integrated parallel hydrologic model, J. Hydrol., 519, 2238–2257,
1399   doi:10.1016/J. Hydrol.2014.10.020, 2014.
1400   Steefel, C. I., and Yabusaki, S. B.: OS3D/GIMRT software for modeling multicomponent-
1401   multidimensional reactive transport, Richland, WA, 1996.
1402   Steefel, C. I.: CrunchFlow Software for Modeling Multicomponent Reactive Flow and Transport
1403   User's Manual, 2009.
1404   Steefel, C. I., and Van Cappellen, P.: A new kinetic approach to modeling water-rock interaction:
1405   The role of nucleation, precursors, and Ostwald ripening, Geochim. Cosmochim. Acta,
1406   54(10), 2657–2677, doi:10.1016/0016-7037(90)90003-4, 1990.
1407   Steefel, C. I., and Lasaga, A. C.: A coupled model for transport of multiple chemical species and
1408   kinetic precipitation/dissolution reactions with application to reactive flow in single phase

Geoscientific
Model Development
Discussions

1409   hydrothermal systems, Am. J. Sci., 294(5), 529–592, doi:10.2475/ajs.294.5.529, 1994.
1410 Steefel, C. I. et al.: Reactive transport codes for subsurface environmental simulation, Comput.
1411   Geosci., 19(3), 445–478, doi:10.1007/s10596-014-9443-x, 2015.
1412 Steiner, A. L., Pal, J. S., Giorgi, F., Dickinson, R. E., and Chameides, W. L.: The coupling of the
1413   Common Land Model (CLM0) to a regional climate model (RegCM), Theor. Appl.
1414   Climatol., 82(3–4), 225–243, doi:10.1007/s00704-005-0132-5, 2005.
1415 Steiner, A. L., Pal, J. S., Rauscher, S. A., Bell, J. L., Diffenbaugh, N. S., Boone, A., Sloan, L. C.,
1416   and Giorgi, F.: Land surface coupling in regional climate simulations of the West African
1417   monsoon, Clim. Dyn., 33(6), 869–892, doi:10.1007/s00382-009-0543-6, 2009.
1418 Sudicky, E. A., Jones, J. P., Park, Y. J., Brookfield, A. E., and Colautti, D.: Simulating complex
1419   flow and transport dynamics in an integrated surface-subsurface modeling framework,
1420   Geosci. J., 12(2), 107–122, doi:10.1007/s12303-008-0013-x, 2008.
1421 Sulis, M., Meyerhoff, S. B., Paniconi, C., Maxwell, R. M., Putti, M., and Kollet, S. J.: A
1422   comparison of two physics-based numerical models for simulating surface water-
1423   groundwater interactions, Adv. Water Resour., 33(4), 456–467,
1424   doi:10.1016/j.advwatres.2010.01.010, 2010.
1425 Sulis, M., Williams, J. L., Shrestha, P., Diederich, M., Simmer, C., Kollet, S. J., and. Maxwell,
1426   R. M.: Coupling Groundwater, Vegetation, and Atmospheric Processes: A Comparison of
1427   Two Integrated Models, J. Hydrometeorol., 18(5), 1489–1511, doi:10.1175/JHM-D-16-
1428   0159.1, 2017.
1429 Therrien, R and Sudicky, E.: Three-dimensional analysis of variably-saturated flow and solute
1430   transport in discretely- fractured porous media, J. Contam. Hydrol., 23(95), 1–44,
1431   doi:10.1016/0169-7722(95)00088-7, 1996.
1432 Tompson, A. F. B., Ababou, R., and Gelhar, L. W.: Implementation of the three-dimensional
1433   turning bands random field generator, Water Resour. Res., 25(10), 2227–2243,
1434   doi:10.1029/WR025i010p02227, 1989.
1435 Tompson, A. F. B., Ashby, S. F., and Falgout, R. D.: Use of high performance computing to
1436   examine the effectiveness of aquifer remediation, 1994.
1437 Tompson, A. F. B., Falgout, R. D., Smith, S. G., Bosl, W. J., and Ashby, S. F.: Analysis of
1438   subsurface contaminant migration and remediation using high performance computing,
1439   Adv. Water Resour., 22(3), 203–221, doi:10.1016/S0309-1708(98)00013-X, 1998.
1440 Tompson, A. F. B., Carle, S. F., Rosenberg, N. D., and Maxwell, R. M.: Analysis of
1441   groundwater migration from artificial recharge in a large urban aquifer: A simulation
1442   perspective, Water Resour. Res., 35(10), 2981–2998, doi:10.1029/1999WR900175, 1999.
1443 Valcke, S.: The OASIS3 coupler : a European climate modelling community software, Geosci.
1444   Model Dev, 6, 373–388, doi:10.5194/gmd-6-373-2013, 2013.
1445 Valcke, S., Balaji, V., Bentley, P., Guilyardi, E., Lawrence, B., and Pascoe, C.: Developing a
1446   Common Information Model for climate models and data, Geophys. Res. Abstr., 11, 10592,
1447   2009.
1448 Valcke, S., Balaji, V., Craig, A., Deluca, C., Dunlap, R., Ford, R. W., Jacob, R., Larson, J., and
1449   Kuinghttons, O. R.: Model Development Coupling technologies for Earth System
1450   Modelling, Geosci. Model Dev., 5, 1589–1596, doi:10.5194/gmd-5-1589-2012, 2012.
1451 VanderKwaak, J. E.: Numerical simulation of flow and chemical transport in integrated surface-
1452   subsurface hydrologic systems, 1999.
1453 VanGenuchten, M. T.: A Closed-form Equation for Predicting the Hydraulic Conductivity of
1454   Unsaturated Soils, Soil Sci. Soc. Am. J., 44, 892–898,

Geoscientific
Model Development
Discussions

1455   doi:10.2136/sssaj1980.03615995004400050002x, 1980.

1456 Visbal, M., and Knight, D.: Generation of orthogonal and nearly orthogonal coordinates with
1457   gridcontrol near boundaries, AIAA J., 20(3), 305–306, doi:10.2514/3.7915, 1982.

1458 Vogel, B., Vogel, H., Bangert, M., Lundgren, K., Rinke, R., and Stanelle, T.: The comprehensive
1459   model system COSMO-ART – Radiative impact of aerosol on the state of the atmosphere
1460   on the regional scale, Atmos. Chem. Phys., 9, 8661–8680, 2009.

1461 Volker, J.: Multigrid Methods, , doi:10.1137/1.9781611971057, 1987.

1462 Wagner, S., Fersch, B., Yuan, Y.,Yu, Z., and Kunstmann, H.: Fully coupled atmospheric-
1463   hydrological modeling at regional and long-term scales: Development, application, and
1464   analysis of WRF-HMS, Water Resour. Res., 52(4), 3187–3211,
1465   doi:10.1002/2015WR018185, 2016.

1466 Weill, S., Mouche, E., and Patin, J.: A generalized Richards equation for surface/subsurface flow
1467   modelling, J. Hydrol., 366(1–4), 9–20, doi:10.1016/j.jhydrol.2008.12.007, 2009.

1468 Weill, S., Mazzia, A., Putti, M., and Paniconi, C.: Coupling water flow and solute transport into
1469   a physically-based surface-subsurface hydrological model, Adv. Water Resour., 34(1), 128–
1470   136, doi:10.1016/j.advwatres.2010.10.001, 2011.

1471 Williams, J. L., and Maxwell, R. M.: Propagating Subsurface Uncertainty to the Atmosphere
1472   Using Fully Coupled Stochastic Simulations, J. Hydrometeorol., 12(1994), 690–701,
1473   doi:10.1175/2011JHM1363.1, 2011.

1474 Williams, J. L., Maxwell, R. M., and Monache, L. D.: Development and verification of a new
1475   wind speed forecasting system using an ensemble Kalman filter data assimilation technique
1476   in a fully coupled hydrologic and atmospheric model, J. Adv. Model. Earth Syst., 5(4), 785–
1477   800, doi:10.1002/jame.20051, 2013.

1478 Wood, B. D.: The role of scaling laws in upscaling, Adv. Water Resour., 32(5), 723–736,
1479   doi:10.1016/j.advwatres.2008.08.015, 2009.

1480 Woodward, S. C.: A Newton-Krylov-multigrid solver for variably saturated flow problems,
1481   Proceedings on the Twelfth International Conference on Computational Methods in Water
1482   Resources, in Computational Mechanics Publications, vol. 2, pp. 609–616, 1998.

1483 Xu, L., Raman, S., and Madala, R. V.: A review of non-hydrostatic numerical models for the
1484   atmosphere, Math. Subj. Classif, 1991.

1485 Xue, M., Droegemeier, K. K., and Wong, V.: The Advanced Regional Prediction System
1486   (ARPS) - A multi-scale nonhydrostatic atmospheric simulation and prediction tool. Part II:
1487   Model dynamics and verification, Meteorol. Atmos. Phys., 75, 161–193,
1488   doi:10.1007/s007030170027, 2000.

1489 Zhufeng F., Bogena, H., Kollet, S., Koch, J. H. V.: Spatio-temporal validation of long-term 3D
1490   hydrological simulations of a forested catchment using empirical orthogonal functions and
1491   wavelet coherence analysis, Hydrology, 529(1754–1767), 2015.

1492